Sedimentology (2004) **51,** 1029–1051 doi: 10.1111/j.1365-3091.2004.00659.x

Multistage hydrothermal dolomites in the Middle Devonian (Givetian) carbonates from the Guilin area, South China

DAIZHAO CHEN*, HAIRUO QING† and CHAO YANG†
*Institute of Geology and Geophysics, Chinese Academy of Sciences, PO Box 9825, Beijing 100029, China (E-mail: dzh-chen@mail.igcas.ac.cn)
†Department of Geology, University of Regina, Regina, SK, Canada S4S 0A2 (E-mail: hairuo.qing@uregina.ca)

ABSTRACT

Pervasive dolomites occur preferentially in the stromatoporoid biostromal (or reefal) facies in the basal Devonian (Givetian) carbonate rocks in the Guilin area, South China. The amount of dolomites, however, decreases sharply in the overlying Frasnian carbonate rocks. Dolostones are dominated by replacement dolomites with minor dolomite cements. Replacement dolomites include: (1) fine to medium, planar-e floating dolomite rhombs (Rd1); (2) medium to coarse, planar-s patchy/mosaic dolomites (Rd2); and (3) medium to very coarse non-planar anhedral mosaic dolomites (Rd3). They post-date early submarine cements and overlap with stylolites. Two types of dolomite cements were identified: planar coarse euhedral dolomite cements (Cd1) and non-planar (saddle) dolomite cements (Cd2); they post-date replacement dolomites and predate late-stage calcite cements that line mouldic vugs and fractures. The replacement dolomites have $\delta^{18}O$ values from −13·7 to −9·7‰ VPDB, $\delta^{13}C$ values from −2·7 to + 1·5‰ VPDB and $^{87}Sr/^{86}Sr$ ratios from 0·7082 to 0·7114. Fluid inclusion data of Rd3 dolomites yield homogenization temperatures (T_h) of 136–149 °C and salinities of 7·2–11·2 wt% NaCl equivalent. These data suggest that the replacive dolomitization could have occurred from slightly modified sea water and/or saline basinal fluids at relatively high temperatures, probably related to hydrothermal activities during the latest Givetian–middle Fammenian and Early Carboniferous times. Compared with replacement dolomites, Cd2 cements yield lower $\delta^{18}O$ values (−14·2 to −9·3‰ VPDB), lower $\delta^{13}C$ values (−3·0 to −0·7‰ VPDB), higher $^{87}Sr/^{86}Sr$ ratios (≈ 0·7100) and higher T_h values (171–209 °C), which correspond to trapping temperatures (T_r) between 260 and 300 °C after pressure corrections. These data suggest that the dolomite cements precipitated from higher temperature hydrothermal fluids, derived from underlying siliciclastic deposits, and were associated with more intense hydrothermal events during Permian–Early Triassic time, when the host dolostones were deeply buried. The petrographic similarities between some replacement dolomites and Cd2 dolomite cements and the partial overlap in $^{87}Sr/^{86}Sr$ and $\delta^{18}O$ values suggest neomorphism of early formed replacement dolomites that were exposed to later dolomitizing fluids. However, the dolomitization was finally stopped through invasion of meteoric water as a result of basin uplift induced by the Indosinian Orogeny from the early Middle Triassic, as indicated by the decrease in salinities in the dolomite cements in veins (5·1–0·4 wt% NaCl equivalent). Calcite cements generally yield the lowest $\delta^{18}O$ values (−18·5 to −14·3‰ VPDB), variable $\delta^{13}C$ values (−11·3 to −1·2‰ VPDB) and high T_h values (145–170 °C) and low salinities (0–0·2 wt% NaCl equivalent), indicating an origin of high-temperature, dilute fluids recharged by meteoric water in the course of basin uplift during the Indosinian Orogeny. Faults were

probably important conduits that channelled dolomitizing fluids from the deeply buried siliciclastic sediments into the basal carbonates, leading to intense dolomitization (i.e. Rd3, Cd1 and Cd2).

Keywords China, Devonian, diagenesis, dolomitization, hydrothermal fluids.

INTRODUCTION

Pervasive dolomites occur in the Middle Devonian (Givetian) carbonate rocks, especially in the basal unit that overlies the Pragian–Eifelian siliciclastic rocks in the Guangxi–Hunan region, South China. Dolomitization locally obliterated original depositional textures, leading to many uncertainties in stratigraphic correlations. The stratigraphic equivalents of these rocks are important host rocks for large-scale Pb–Zn and polymetallic deposits in South China (e.g. Shen *et al.*, 1987; Wu *et al.*, 1987; Chen & Gao, 1988; Han & Hutchinson, 1990; Chen *et al.*, 1998). Thus, an understanding of the origins of the dolomite can provide important information on the evolution of basinal fluids, fluid–rock interactions during diagenesis and processes of mineralization, which, in turn, can further improve mining and exploration strategies.

In the absence of detailed studies, the mechanism of dolomitization in these Devonian carbonate rocks is poorly understood. Based on the presence of vugs and vuggy calcite cements, some researchers (e.g. Shen *et al.*, 1994; Du *et al.*, 1996; Gong *et al.*, 1997) assumed that these dolomites might have formed in relation to subaerial exposure (or karstic process) soon after deposition.

In order to characterize the massive dolostones in the Middle Devonian carbonates in the Guilin area, selected outcrops were studied with an emphasis on petrographic features and vertical and lateral distributions of the dolomites. Thin section and cathodoluminescence microscopy studies were also carried out to establish the diagenetic paragenesis of the dolomite. Oxygen and carbon isotopes, strontium isotopes and fluid inclusion microthermometry were performed in order to obtain geochemical signatures of these dolomites and their parental fluids. This study provides an example of multistage dolomitization in the Devonian strata of South China, related to the well-documented hydrothermal activities there during Middle to Late Palaeozoic time (e.g. Gou, 1985; Wu *et al.*, 1987; Jin, 1990; Zhou, 1990; Zhong *et al.*, 1992; Liu *et al.*, 1993; Chen *et al.*, 1994; Feng *et al.*, 1997, 1998; Chen *et al.*, 2001a, 2002). The focus of this study is on the basal Givetian carbonates in both platformal and basinal successions in the Guilin area. From the gathered data, a conceptual model for dolomitization is then proposed.

GEOLOGICAL SETTING

Depositional setting and stratigraphy

From late Middle Devonian (Givetian) time, the progressive north-eastward marine transgression from southern Guangxi led to the onset of carbonate deposition in the Guilin area and expansion to the Hunan Province farther north (e.g. Shen *et al.*, 1987; Wu *et al.*, 1987; Chen *et al.*, 2001a,b). In the Devonian sea realm of South China, two elongate basins trending NNE–SSW existed and extended curvilinearly for about 800 km from the Guangxi to Hunan provinces. These were interpreted as having been formed through strike-slip rifting reactivated along antecedent basement fault zones (Zeng *et al.*, 1992; Liu *et al.*, 1993; Chen *et al.*, 2001a). They intersected two *en echelon* basins trending NE–SW in Guangxi and a rhomb-shaped basin trending approximately NW–SE in southern Hunan. Carbonate platforms were developed on the palaeohighs separated by these basins (Fig. 1).

The Guilin Platform was circumscribed by a series of interplatformal basins and was bridged to a larger platform farther east through a narrow platform (Fig. 1B). A spindle- to rhomb-shaped Yangshuo Basin appeared to the east of this platform (Fig. 1). Such a carbonate platform–basin configuration was proposed to have been formed in relation to secondary sinistral strike-slip faulting, induced by the major basement strike-slip faulting that initiated in the late Givetian and culminated in the early Frasnian (Chen *et al.*, 2001a, 2002). This strike-slip faulting resulted in intense hydrothermal activity, leading to deposition of extensive bedded chert, interbedded with tuffaceous partings, in the interplatformal basin of South China (Chen *et al.*, 2001a).

A summary of stratigraphic units and their distributions from platform interior to intraplatformal basin is illustrated in Fig. 2, and relevant

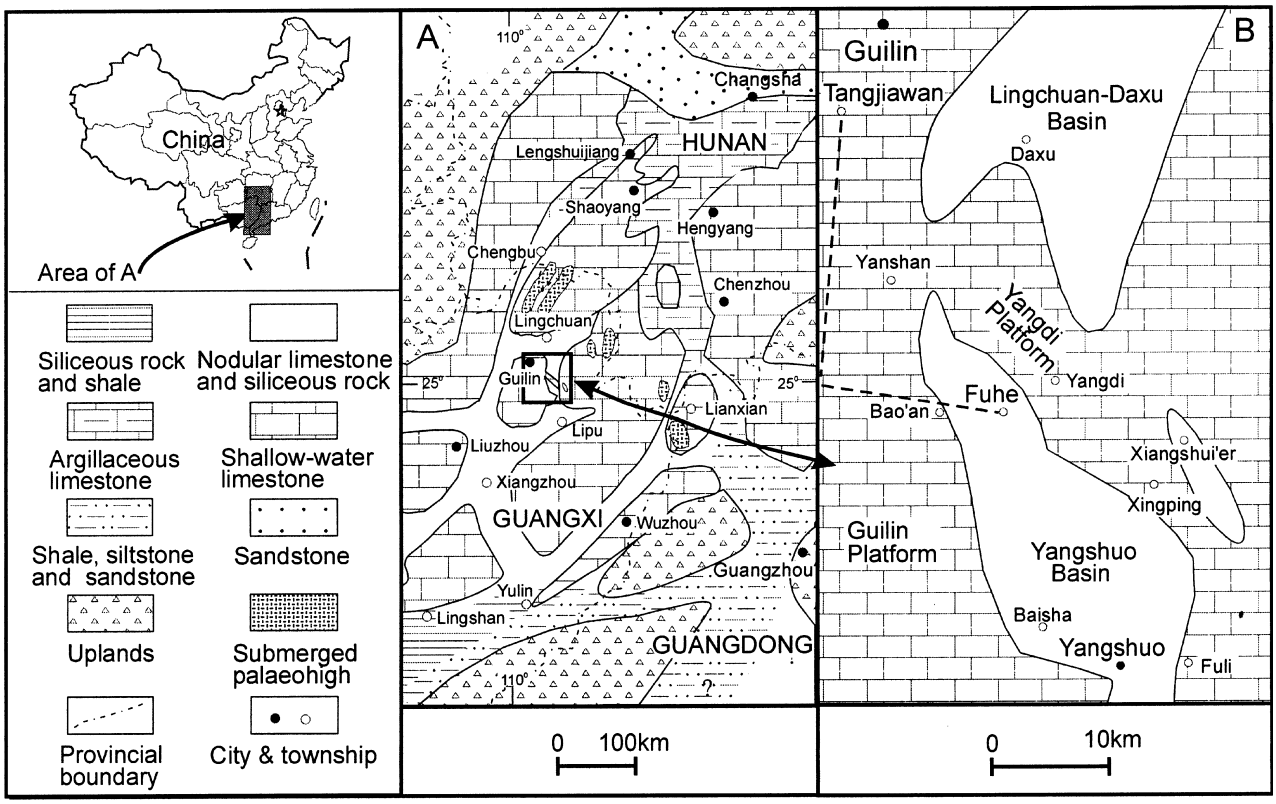

Fig. 1. Palaeogeographic setting of Guangxi and Hunan provinces in the Givetian–Frasnian (A) and detailed platform–basin configuration of Guilin region (B). Dashed lines in (B) show the location of the schematic stratigraphic cross-section illustrated in Fig. 2.

information can also be found in Zhong *et al.* (1992) and Chen *et al.* (2001a, 2002). A siliciclastic succession, 1100–1700 m thick, underlies the carbonate strata and unconformably overlies the metamorphosed Cambrian (locally Ordovician) flysch assemblages. These siliciclastic deposits, spanning from Pragian to Eifelian in age, are dominated by argillaceous successions, with subordinate sandy sediments deposited in coastal to shelf environments (Wu *et al.*, 1987; Zhong *et al.*, 1992). The Devonian carbonate rocks include the following formations: Tangjiawan, Guilin, Rongxian, Mintang, Liujiang and Gubi; the focus of this study is the Tangjiawan Formation and the Lower Member of the Guilin Formation, in which extensive dolomites are present.

The Tangjiawan Formation is the first carbonate succession overlying the siliciclastic deposits and is dominated by dolomitized stromatoporoid biostromal and/or reefal facies, with minor open-marine facies in the intrashelf basin (Fig. 2). The Guilin Formation is dominated by stromatoporoid biohermal facies with subordinate intertidal microbial laminites, but is barren of supratidal laminites. The Rongxian Formation is characterized by creamy white oncoidal–peloidal packstones/grainstones and microbial rudstones. The Mintang Formation consists of interfingering of deep-water microbial laminites and thin-bedded lime mudstones/wackestones with planktonic tentaculitids. The Liujiang Formation (mainly Frasnian) is composed of two parts: the lower thin-bedded cherty lime mudstones rich in organic matter and pelagic fauna; and the upper bedded cherts interbedded with tuffaceous chert. The Gubi Formation consists of megabreccias and calciturbidites on the marginal slope and calciturbidites and pelagic limestones in the basin centre.

Burial history and major post-depositional events

Carbonate deposition initiated over the siliciclastic successions during Givetian time. The basal Devonian carbonate rocks were then buried to a depth of 5·5–7 km during the Late Permian–Early Triassic (Fig. 3). However, they were folded/faulted and quickly uplifted in the Middle Triassic as a result of the Indosinian Orogeny (Fig. 3) (e.g. GMRBG, 1988, 1994; Liu *et al.*, 1993). At

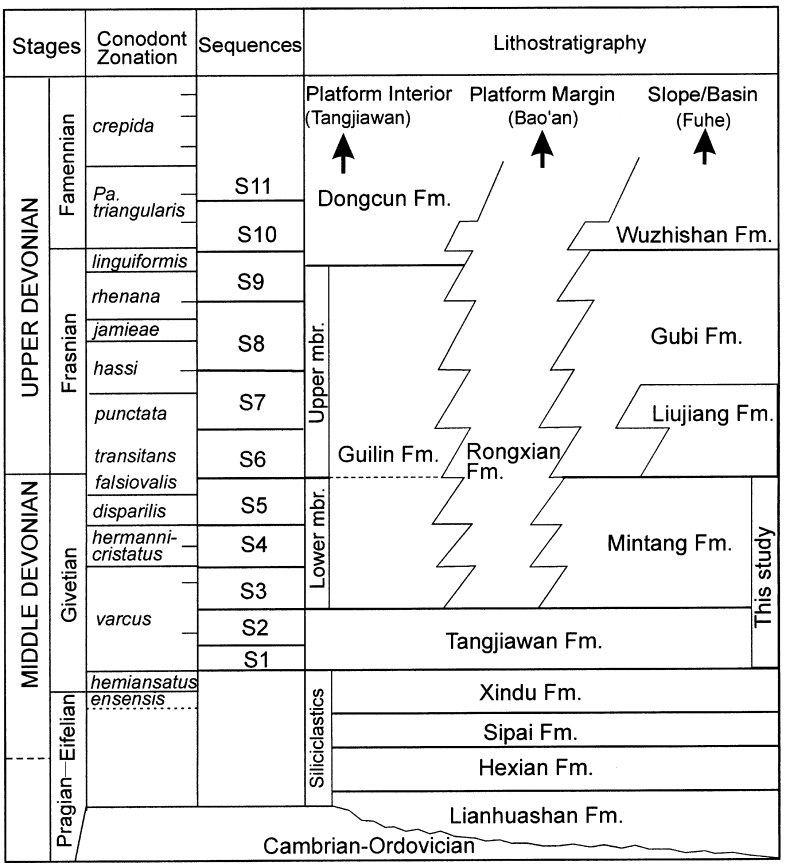

Fig. 2. Lithostratigraphic relationships and nomenclature for the Devonian platform and basinal successions in Guilin area. Depositional sequences are documented in Chen *et al.* (2001a, 2002).

present, only Devonian to Lower Carboniferous successions are preserved in the study area because of persistent erosion in response to the later Yanshanian and Himalayan orogenies (Late Jurassic to Present).

Four major episodes of hydrothermal and/or tectonic events took place in South China after the burial of the basal carbonates (Fig. 3). The earliest hydrothermal activity occurred from the latest Givetian to middle Famennian time during shallow burial of the basal carbonates. This hydrothermal event was characterized by bedded cherts intercalated with tuffaceous partings or local pillow lavas in the interplatformal basins (Wu *et al.*, 1987; Jin, 1990; Zhou, 1990; Zhong *et al.*, 1992; Chen *et al.*, 2001a, 2002). The second hydrothermal event occurred from the late Tournaisian to Viséan during the Early Carboniferous (the Early Hercynian Movement; Wang, 1985) and was characterized by bedded cherts (or siliceous shales) and pyroclastic and eruptive rocks in the basins bounded by deep-seated faults (Chen *et al.*, 1994; Feng *et al.*, 1998). The third episode was most active during the transition between the Early and Late Permian and was characterized by extensive basalts over platforms, diabase intrusions (south-western China mostly) and/or block uplift (Dongwu or Late Hercynian Orogeny; Wang, 1985; Sha *et al.*, 1990; Wang *et al.*, 1994). The fourth episode was characterized by hydrothermal (or volcanic) activities intermittently occurring from the latest Permian until the basin inversion starting from the Early Middle Triassic (Indosinian Orogeny) (Fig. 3; Gou, 1985; Liu *et al.*, 1993; Feng *et al.*, 1997). The Devonian strata were subsequently exhumed during the Middle Triassic, leading to the onset of karstification, as demonstrated by the spectacular tower karstic scenery today in the study area. During this period of time, meteoric water may have been flushed downwards into the Devonian strata. During the Late Triassic, continental lakes were developed in fault-controlled, NE- to SW-trending depressions or sags; lake deposits of that time unconformably overlie the Upper Devonian carbonates locally (GMRBG, 1988, 1994).

The deep-seated syndepositional strike-slip fault zones were also reactivated later when the Devonian strata were buried deeply during the Early (Early Carboniferous) and Late (Late Permian) Hercynian tectonic episodes (e.g. Wang, 1985) and the Indosinian Orogeny. The measured

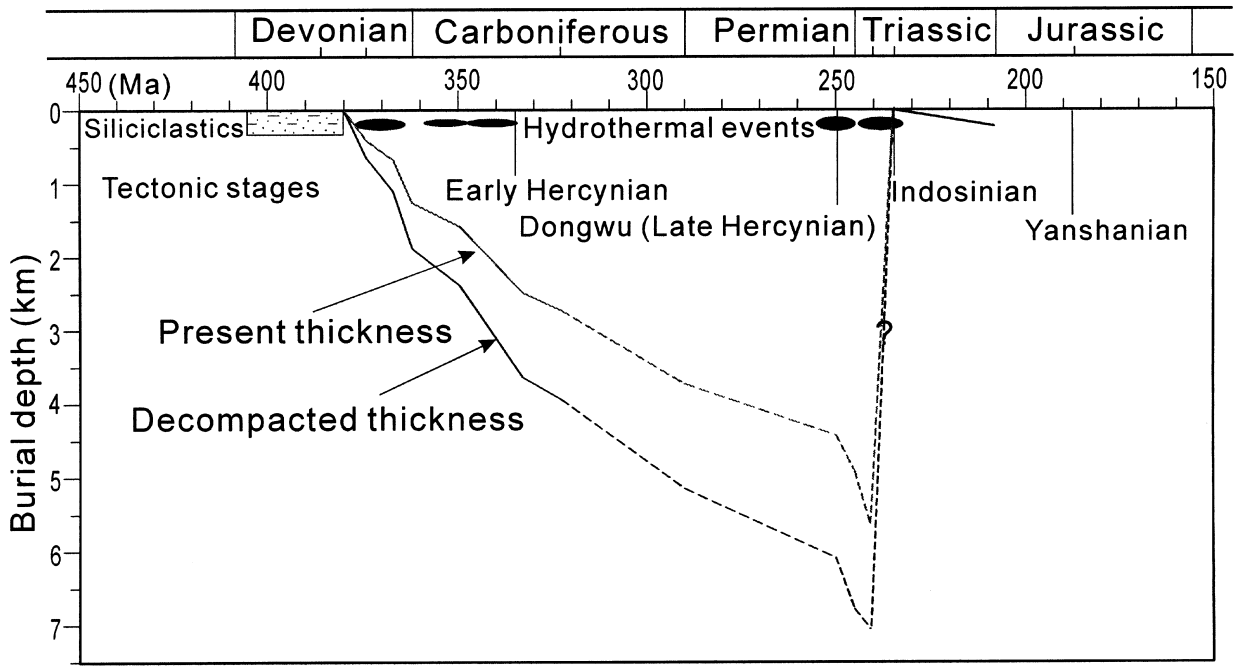

Fig. 3. Burial history of Devonian basal carbonates (Tangjiawan Formation) in the Guilin area, with maximum burial of about 5·5–7·0 km in the Early Triassic and exhumation in the Middle Triassic. The curve is constructed using the method proposed by Doglioni & Goldhammer (1988) and Goldhammer (1997). The solid part of the curve represents preserved rock sequences with thickness data based on GMRBG (1988, 1994), and the dashed part represents lately eroded rock sequences with thickness data based on Wang (1985) and Sha *et al.* (1990) from neighbouring regions. Several episodes of hydrothermal anomalies (black nodules) took place from shallow to deepest burial of Givetian carbonates and exerted fundamental controls on dolomitization.

sections in this study are adjacent to the large-scale fault zones formed during the Indosinian Orogeny (cf. GMRBG, 1988, 1994; Chen *et al.*, 2001a). These fault/fracture zones probably acted as fluid conduits, through which the basement-derived fluids migrated upwards into the basal carbonate strata during hydrothermal activities (see later discussion).

RESEARCH METHODS

Two outcrop sections at Fuhe and Tangjiawan in the Guilin area were mapped in detail (Fig. 1b), which represent basinal and platformal successions respectively. At both localities, about 500–2500 m of carbonate sections from the Givetian to Lower Carboniferous were preserved and exposed; the occurrence of different types of dolomite, their relative abundance, the vertical and lateral distribution and the lithofacies of the host carbonates were logged at the outcrops. Detailed petrographic studies were conducted on hand specimens and thin sections that were stained with Alizarin Red-S and potassium ferricyanide (Dickson, 1965) to distinguish calcite from dolomite and ferroan carbonate from non-ferroan carbonate. Cathodoluminescence (CL) microscopy was performed on a CL8200MK4 stage from Cambridge Image Technology, using a gun current of 320–350 μA at 12–15 kV.

Different types of dolomite and calcite were sampled using a microdrilling device for carbon and oxygen isotope analysis ($n = 35$) and strontium isotope analysis ($n = 26$), which were performed at the University of Saskatchewan, Canada. For C and O isotope analysis, about 100 μg of samples was reacted with anhydrous phosphoric acid for 200 s at 70 °C in a Finnigan Kiel-III carbonate preparation device coupled to the inlet of a Finnigan MAT-253 mass spectrometer. The $\delta^{13}C$ and $\delta^{18}O$ values are reported in per mil relative to the Vienna Peedee Belemnite (VPDB) standard. Precision of measurements was monitored through routine analyses of NBS-18 and NBS-19 standards, and the standard deviation was better than $\pm 0{\cdot}1‰$ (1σ) for both $\delta^{13}C$ and $\delta^{18}O$. For strontium isotope analyses, 50–100 mg of sample powders was dissolved in 2·5 N HCl, and the strontium was then extracted using the conventional cation exchange procedures. The $^{87}Sr/^{86}Sr$ ratios were measured on a Finnigan

Table 1. Isotopic data ($\delta^{13}C$, $\delta^{18}O$ and $^{87}Sr/^{86}Sr$) of epigenetic carbonates in the Givetian, Guilin area

Location	Sample	Lithology	$\delta^{13}C$ (‰ VPDB)	$\delta^{18}O$ (‰ VPDB)	$^{87}Sr/^{86}Sr$ (± 2σ)
Fuhe	FH3a	Rd2 dolomite	−0·05	−10·50	
	FH3a*	Repeated run	−0·06	−10·55	
	FH3b	Rd2 dolomite	−0·14	−10·93	0·709876 ± 05
	FH3c	Dolomitic limestone	0·45	−16·63	
	FHD1-md	Rd3-m dolomite	−0·64	−10·68	
	FHD1-cd	Rd3-c dolomite	−0·54	−10·94	0·708423 ± 10
	FHD1-s	Vein Cd2 dolomite	−1·35	−11·18	0·708625 ± 10
	FHD1-s1	Vuggy Cd2 dolomite	−0·69	−11·14	
	FHD1-dc	Rd2 dolomite	−0·68	−10·48	0·708493 ± 05
	FHD2-cd	Rd3-c dolomite	−2·72	−11·77	0·711379 ± 04
	FHD2-s	Cd2 lining Rd3 breccias	−2·37	−12·76	0·711239 ± 10
	FHD2-c	Vein calcite lining Cd2 (Stage 1)	−11·29	−15·42	0·709573 ± 05
	FHD3-c	Vuggy calcite (Stage 1)	−4·05	−17·11	
	FHD5-cd	Rd3-c dolomite	−0·03	−10·33	0·708296 ± 05
	FHD5-s	Vuggy Cd2 dolomite	−1·48	−11·06	0·709867 ± 04
Tangjiawan	TJB2-cd	Rd3-c dolomite	1·54	−9·74	0·708419 ± 05
	TJB2-cd*	Repeated run	1·48	−9·74	
	TJB2-s	Vuggy Cd2 dolomite	−1·27	−9·28	
	TJB2-c	Vuggy calcite lining Cd2 (Stage 1)	−9·75	−6·24	0·707895 ± 04
	TJB3-d1	Dolomitic limestone	−0·19	−12·10	0·708235 ± 05
	TJB3-ca1	Vein calcite trending NW–SE (Stage 1)	−1·21	−16·94	0·707986 ± 05
	TJB3-ca2	Vein calcite in the centre (Stage 1)	−1·27	−17·05	
	TJB4-d1	Dolomitic limestone	−0·75	−10·48	0·707996 ± 06
	TJB4-c	Vein calcite trending NE–SW (Stage 2)	−3·72	−17·74	0·709910 ± 15
	TJB5-cd	Rd3-c dolomite	0·89	−12·70	0·710574 ± 04
	TJB5-s	Vuggy Cd2 dolomite	−2·95	−14·23	0·710649 ± 05
	TJB5-dc	Vuggy Cd2 dolomite	−1·68	−13·81	0·710650 ± 03
	TJB5-c	Vuggy calcite (Stage 1)	−8·72	−14·30	0·709074 ± 05
	TJB6-md	Rd3-m dolomite	0·28	−10·25	
	TJB6-cd	Rd3-c dolomite	0·18	−10·02	0·708213 ± 14
	TJB6-s	Vuggy Cd2 dolomite	−1·05	−10·52	0·709638 ± 06
	TJB6-dc	Rd2 dolomite	−0·76	−10·28	0·708326 ± 06
	TJB6-c	Vuggy calcite (Stage 1)	−1·78	−15·18	0·709456 ± 07
	TJB7-md	Rd3-m dolomite	0·23	−9·88	0·708939 ± 07
	TJB8-c	Vein calcite trending NW–SE (Stage 1)	−2·46	−18·53	0·708180 ± 06
	TJ9	Rd3-m dolomite	0·44	−13·68	0·708679 ± 31#
	TJGL40	Rd3-c dolomite	0·25	−11·08	

Rd3-m, -c, medium- and coarse-crystalline Rd3 dolomite respectively.
Not enough for repeated run.

MAT-261 mass spectrometer. The $^{87}Sr/^{86}Sr$ ratios are corrected relative to the NBS987 standard. The analytical mean error (2σ) is $\pm 6{\cdot}4 \times 10^{-6}$ for $^{87}Sr/^{86}Sr$ ratios (Table 1).

A fluid inclusion petrographic study was carried out on selected doubly polished thin sections to determine the properties of fluids responsible for different epigenetic carbonates. In order to minimize the effect of re-equilibration (e.g. stretching, leaking and necking) on the homogenization temperatures (T_h), the fluid inclusion assemblage (FIA), defined as a group of inclusions along a single growth zone with consistent vapour/liquid ratios (Goldstein & Reynolds, 1994), was applied for microthermometric measurement. Microthermometric analysis was carried out on a Fluid Inc. gas flow, heating–cooling stage. The accuracy of final melting temperature of ice (T_m) and T_h values is within 0·3 and 3 °C respectively. T_m values were used to calculate salinity expressed as wt% NaCl equivalent (Bodnar, 1993): wt% NaCl $= 1{\cdot}78 \times T_m - 0{\cdot}0442 \times T_m^2 + 0{\cdot}000557 \times T_m^3$.

OCCURRENCE OF DOLOMITE AND CALCITE

Pervasive dolomites are present mainly in the Givetian carbonate rocks, especially in the basal

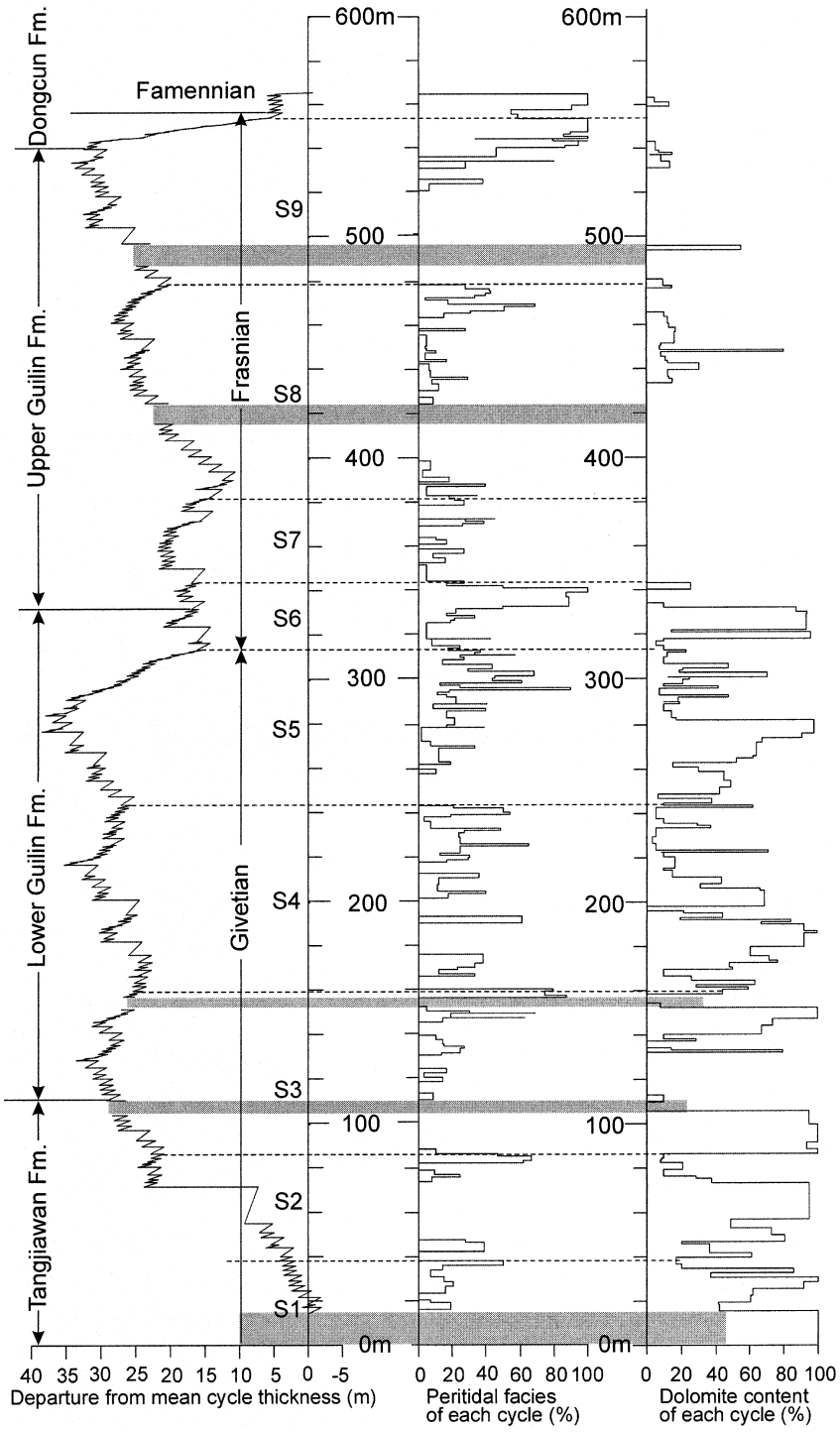

Fig. 4. Dolomite distribution in the Givetian and Frasnian carbonates at Tangjiawan (see Fig. 1 for location). A sharp decrease in dolomite content is apparent in the Frasnian strata and above. The curve on the left is constructed using the Fischer plot technique to demonstrate short- to long-term changes in accommodation space (or sea level), based on the cycle thickness. Shaded bars indicate covered intervals in the field.

Tangjiawan Formation, and the amount of dolomite decreases drastically in the overlying carbonate strata from the Frasnian, both in platform (upper Guilin Formation) (Fig. 4) and basinal successions (Liujiang and Gubi Formation) (Fig. 5). Dolomitization occurred preferentially in stromatoporoid biostromal/reefal facies. In contrast, the peritidal facies (microbial laminites) were less affected by dolomitization (Fig. 4). Within stromatoporoid biostromal/reefal facies, dolomitization commonly initiated in the host carbonate matrix, whereas the skeletal organisms/fragments were less affected by dolomitization (Fig. 6A). Dolomitized horizons have a dark grey to black appearance. Minor dolomite cements (saddle dolomites mostly) are present in skeletal

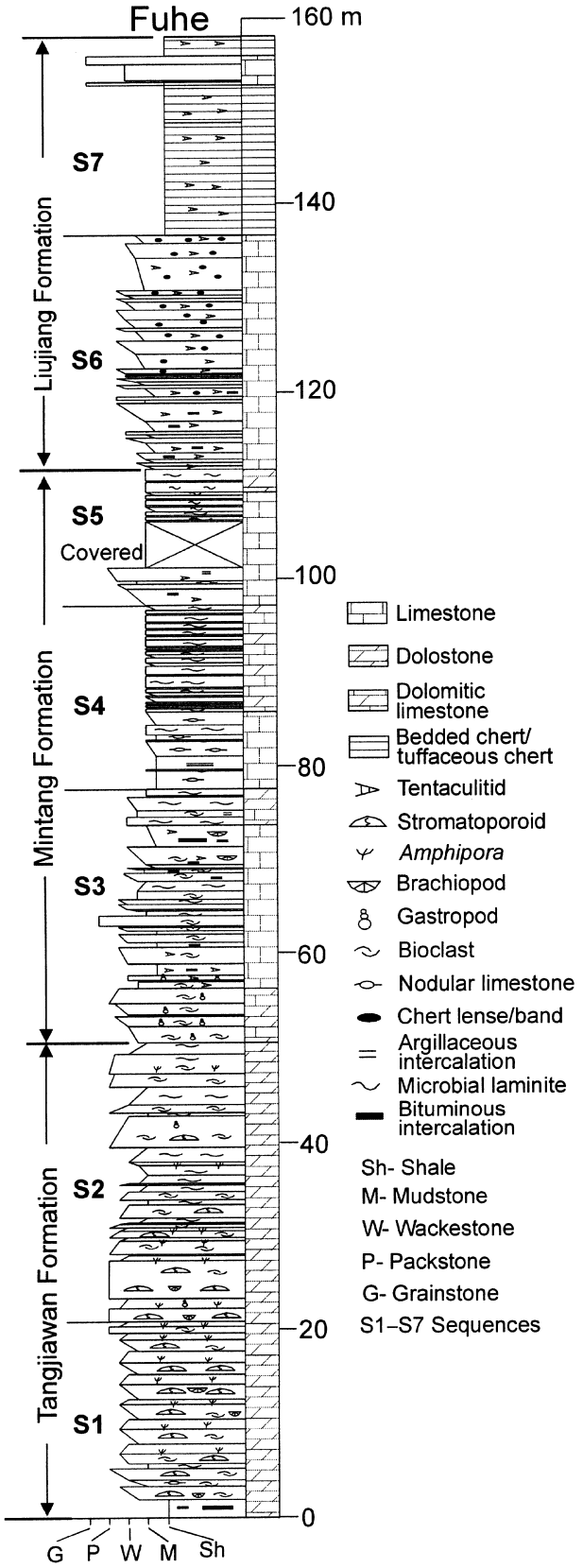

Fig. 5. Stratigraphic distribution of dolomites in the basinal succession at Fuhe. Dolomites occur only in the Givetian strata, especially in the basal carbonates (Tangjiawan Formation), and decrease volumetrically upwards. S1–S7, depositional sequences.

moulds, skeletal chambers, vugs and fractures (Fig. 6B–D). Late-stage, coarse to very coarse crystalline calcite cements are present towards the centre of cavities lined with saddle dolomites and in fractures/veins (Fig. 6C–E).

PETROGRAPHY

Five types of dolomite are recognized, based on the crystal size, distribution and crystal boundary shape (non-planar or planar) (e.g. Sibley & Gregg, 1987; Amthor *et al.*, 1993). They are: (1) fine- to medium-crystalline, planar-e dolomite rhombs (Rd1); (2) coarse-crystalline, planar-s (e), subhedral to euhedral patchy/mosaic dolomites (Rd2); (3) medium- to coarse-crystalline, non-planar, anhedral mosaic dolomites (Rd3); (4) coarse-crystalline, planar-e, euhedral to subhedral dolomite cements (Cd1); and (5) coarse- to very coarse-crystalline, non-planar, saddle dolomite cements (Cd2). Types 1–3 of the dolomite textures are replacive in origin, whereas types 4 and 5 are dolomite cements. Late-stage calcite cements are commonly present in the dolostones. All the dolomites and calcites are non-ferroan, based on the staining.

Replacement dolomites

Rd1 dolomite

The Rd1 dolomite occurs mainly as scattered euhedral to subhedral dolomite crystals, 10–250 μm (commonly 150–200 μm) in size, floating in the host matrix of skeletal wackestones/floatstones, whereas skeletal fragments are less affected by dolomitization (Figs 6A and 7A). The relatively coarse crystals commonly have a cloudy core (euhedral or irregular) with a clear rim exhibiting straight to embayed crystal faces (Fig. 7A). Rd1 dolomite crystals commonly display a sharp extinction under cross-polarized light. Under CL, they show a dull orange-red colour at cores of crystals and a bright orange CL colour towards outer rims. This type of dolomite is commonly present in the argillaceous-rich facies and is more abundant in the basal part of the Tangjiawan Formation. Volumetrically, it only accounts for about 1% (or less) of dolostones.

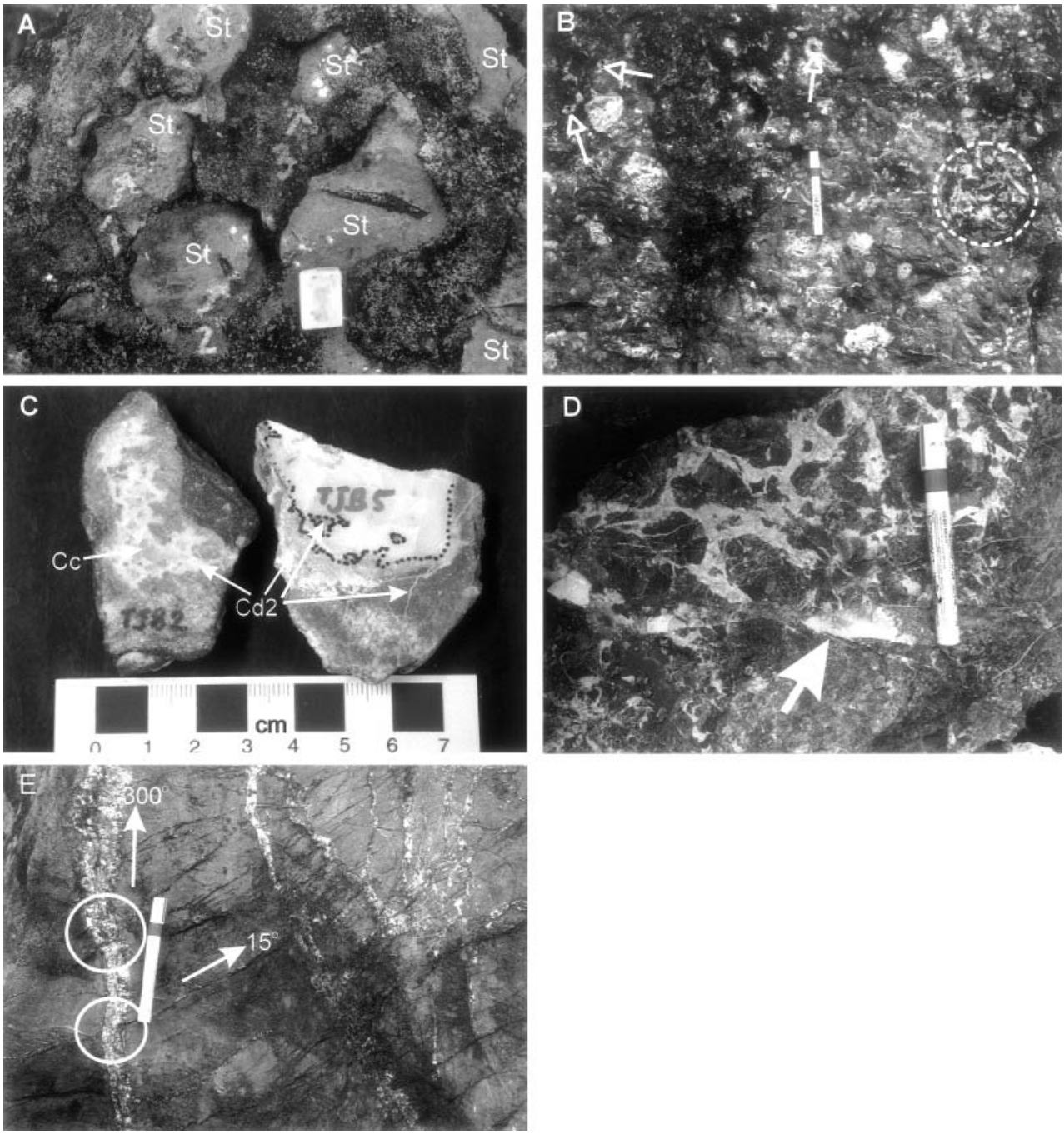

Fig. 6. (A) Photo showing preferentially selective dolomitization in the matrix of stromatoporoid floatstone and weak dolomitization in skeletal stromatoporoids (St). Eraser for scale (2·5 × 3 cm), Tangjiawan Formation, Tangjiawan. (B) Black massive dolostones composed mainly of matrix replacement dolomites with minor dolomite cements (mostly saddle dolomites) lining skeletal mouldic vugs. Note the dolomite breccias lined by dolomite cements (within the circle) and hollow vugs (hollow arrows). Pen for scale (14·5 cm long), Tangjiawan Formation, Tangjiawan. (C) Close-up of creamy-white saddle dolomite cements (Cd2) lining mouldic vugs and fractures (TJB2 and TJB5), which are followed by later stage, very coarse void-filling calcite (Cc). Note the cement breccias within the later calcite fillings (TJB5), Tangjiawan Formation, Tangjiawan. (D) Dark grey to black breccias of matrix replacement dolomites lined with pink-white Cd2 dolomite cements, which are cross-cut by later fracture (see the arrow) filled by calcite cements. Tangjiawan Formation, Fuhe. Pen for scale (14·5 cm long). (E) Field photo showing two sets of late calcite-filled fractures/veins in dolomitic limestones of Tangjiawan Formation, Tangjiawan. Fractures trending NW–SE are cut by those trending NE–SW (within circles). Pen for scale (14·5 cm long).

Rd2 dolomite

The Rd2 dolomite consists of planar-s (e), subhedral dolomite crystals with straight to slightly stepped crystal faces (Fig. 7B–D), which display a homogeneous to weak undulatory extinction. The dolomite crystals commonly have a cloudy core (subhedral or petal-like) with a clear rim. This type of dolomite is characterized by unimodal (bimodal locally) crystal size (150–600 μm) and occurs as sucrosic mosaics/patches in the matrix of the host carbonate rocks. Abundant intercrystalline pore spaces are present and are partially filled with bitumen (mostly pyrobitumen) (Fig. 7C). Under CL, the Rd2 dolomite shows alternating dull and bright orange-red bands (3–5 stages), generally with a bright thin rim where the crystal faces the pore space (Fig. 7D). Interfaces between zones may be planar, embayed or truncated. Similar dolomite textures are described in the hydrothermal Zn–Pb orefield of the Irish Midlands (e.g. Braithwaite & Rizzi, 1997; Wilkinson & Earls, 2000). These Rd2 dolomites generally co-exist with Rd1 within the same horizon. Volumetrically, they account for about 1–2% of dolostones.

Rd3 dolomite

The Rd3 dolomite is the most abundant. It is commonly fabric destructive and strongly obliterated the original depositional or earlier diagenetic features. The Rd3 dolomite consists of medium- to coarsely crystalline dolomite, ranging from 50 μm to 1 mm. Dolomite crystals are nonplanar, anhedral (rarely subhedral) with curved, irregular intercrystalline boundaries. They are commonly tightly packed, with rare intercrystalline pores locally (Fig. 7G and H). Almost all crystals are cloudy in appearance as a result of abundant inclusions with rare clear rims. They commonly exhibit an undulatory extinction and none to extremely dull blotchy CL. This type of dolomite is pervasively distributed in dolomitized horizons of all facies and accounts for about 90% of all dolostones.

Dolomite cements

Cd1 dolomite cement

The Cd1 dolomite cement consists of planar, euhedral to subhedral crystals (250–1000 μm), which generally have a large cloudy core with a thin clear rim (Fig. 8A). All crystals show a sharp extinction. Under CL, clear rims are compositionally zoned with a dull red colour, whereas cloudy cores exhibit none to very dull CL (Fig. 8B). The dolomite crystals precipitated as cements lining dissolution vugs and mouldic pores in Rd3 dolomites, where relict porosity was commonly preserved towards the pore centre (Fig. 8A). The Cd1 dolomite cement accounts for about 1–2% of the dolostones.

Cd2 (saddle) dolomite cement

The Cd2 (saddle) dolomite cement appears as creamy, pink or white non-planar crystals in hand specimens, ranging from 250 μm up to 4 mm in size, with scimitar-like terminations pointing to pore spaces. It has curved or lobate crystal faces and sweeping extinction (Fig. 8C–F). Under CL, Cd2 saddle dolomites exhibit none to dull blotchy orange-red luminescence in the cores, with clear rims displaying brighter luminescent zoning (Fig. 8F). They occur mainly in completely dolomitized intervals as cements (Figs 6B–D and 8C–F), which partially or completely occlude vugs, moulds and/or fractures. Relict porosity towards the pore centre is either open or filled by later stage calcite cements (Figs 6B and C and 8C–E). Volumetrically, they are relatively insignificant, accounting for only 2–5% of dolostones.

Late-stage calcite cements

Late-stage calcite cements consist of equant to columnar crystals up to a few centimetres in size (e.g. Fig. 6C). Under CL, calcite crystals are nonluminescent to very dull red. They occur as cements lining vugs, fractures and/or veins that post-date dolomite cements (Figs 6C–E and 8D). Although these coarse to very coarse calcite cements are widely distributed in the studied carbonates, they are volumetrically of minor importance (< 5%).

PARAGENETIC SEQUENCE

A summary of the paragenetic sequence of dolomites and calcite cements is illustrated in Fig. 9. In completely dolomitized carbonates, most early diagenetic features (e.g. submarine cements) that occurred before burial or at shallow depth were obliterated by dolomitization. Only in partially dolomitized carbonates in the Tangjiawan, lower Guilin and Mintang Formations can evidence be found that replacement dolomites (Rd1–Rd3) post-dated the early-stage diagenetic features such as micrites and fibrous cements. Rd1

replacement dolomites, occurring as dolomite rhombs/blebs scattered in the argillaceous, organic-rich matrix, are the earliest dolomites precipitated during shallow burial before significant stylolitization (Fig. 7A). These dolomite rhombs commonly became the cores (or nuclei) for later dolomite overgrowths (i.e. Rd2; Fig. 7A and C).

The Rd2 dolomites can either overlap or post-date Rd1 dolomites, as reflected by their co-occurrence and the overgrowth relationships (Fig. 7A and C) described earlier. They mostly post-date low-amplitude stylolites along which they occur as crystal patches (Fig. 7B) or clusters, but predate high-amplitude stylolites (Fig. 7C). Both Rd2 and Rd3 dolomite crystals are rimmed with bitumen (Fig. 7C and H), and some dolomite crystals, especially those occurring along the stylolites (or dissolution sutures) with disseminated bitumen and pyrite, display corrosion features (Fig. 7C–F). Rd2 and Rd3 dolomites therefore predate hydrocarbon migration and associated sulphate reduction corrosion. The hydrocarbon migration and related sulphate reduction was followed by chertification, as chert (or microquartz) either occurs along dissolution sutures with pyrite inclusions or cross-cuts the bitumen fillings (Fig. 7E and F). However, the hydrocarbon migration was terminated before the precipitation of Cd1 and Cd2 dolomites because no bitumen is present in the intercrystalline pores between them.

Both Cd1 and Cd2 dolomite cements post-date Rd3 dolomites, as they line vugs or fractures in the Rd3 dolomites (Figs 6B–D and 8). The presence of overgrowth of Cd2 dolomites upon Cd1 indicates the earlier occurrence of the Cd1 type (Fig. 8C and D), similar to the case described by Wendte *et al.* (1998). The remaining porosity of vugs and veins was mostly open (Figs 6B and 8A, C and E), but was locally filled by late-stage calcite cements (Fig. 8D).

Dolomitization was followed by calcite cementation, as indicated by the calcite cements in vugs and veins (Figs 6C–E and 8D), in which vuggy calcite cements predate vein calcite cements (Fig. 8D). There are two sets of late calcite-filled veins/fractures, trending NW–SE and NE–SW respectively. Based on their cross-cutting relationships, the NW- to SE-trending veins predate the NE–SW ones (Fig. 6E). Both cases point to two phases of calcite cementation such that the vuggy calcite and NW- to SE-trending vein calcite are hence grouped as Stage 1 calcite and the NE- to SW-trending vein calcite as Stage 2 calcite.

ISOTOPE GEOCHEMISTRY

Oxygen and carbon isotopes

Thirty-five outcrop samples of dolomitic limestone, dolomite, vuggy calcite and fracture-filling calcite were collected in both Fuhe and Tangjiawan for oxygen and carbon isotope analyses (Table 1; Fig. 10). The Rd1 and Cd1 dolomites are too small to sample for isotopic analyses. There is no apparent systematic variation of the isotopic values in similar petrographic groups between the two localities. All the $\delta^{18}O$ values are very low (< −9‰ VPDB) in comparison with the $\delta^{18}O$ values of calcite precipitated from Middle Devonian sea water (−4 to −6‰ VPDB; cf. Popp *et al.*, 1986). The $\delta^{13}C$ values of dolostones are in the range of −3 to +2‰ VPDB, whereas those of late calcite cements are lower, especially of the vuggy calcite.

The $\delta^{18}O$ and $\delta^{13}C$ values of dolomitic limestones and replacement dolomites (Rd2, Rd3) overlap each other (Fig. 10). The $\delta^{18}O$ and $\delta^{13}C$ values of Rd2 dolomites are relatively consistent, varying from −10·9 to −10·3‰ VPDB (average −10·5‰) and from −0·8 to 0·0‰ VPDB (average −0·4‰) respectively. For Rd3 dolomites, the $\delta^{18}O$ and $\delta^{13}C$ values range from −13·7 to −9·7‰ VPDB (average −11·0‰) and from −2·7 to +1·5‰ VPDB (average −0·01‰), respectively, without identifiable difference between the medium- and coarse-crystalline textures.

The O and C isotopic values of Cd2 (saddle) dolomite cements vary from −14·2 to −9·3‰ VPDB (average −11·7‰) and from −3·0 to −0·7‰ VPDB (average −1·6‰) respectively (Table 1). The isotopic values of dolomite cements are generally lower than those of replacement dolomites, although there is a small overlap between them (Fig. 10).

The $\delta^{18}O$ and $\delta^{13}C$ values of Stage 1 calcite cements can be grouped into two clusters (Fig. 10): one with $\delta^{18}O$ values from −15·4 to −6·2‰ VPDB (average −12·0‰) and $\delta^{13}C$ values from −11·3 to −8·7‰ VPDB (average −9·9‰), which are the lowest $\delta^{13}C$ values in this study (Fig. 10); and another with $\delta^{18}O$ values from −18·5 to −15·2‰ VPDB (average −17·0‰) and $\delta^{13}C$ values from −4·1 to −1·2‰ VPDB (average −2·2‰) (Table 1; Fig. 10). Only one Stage 2 calcite can be sampled for O and C isotopic analyses, which yields values of −17·7 and −3·7‰ VPDB respectively.

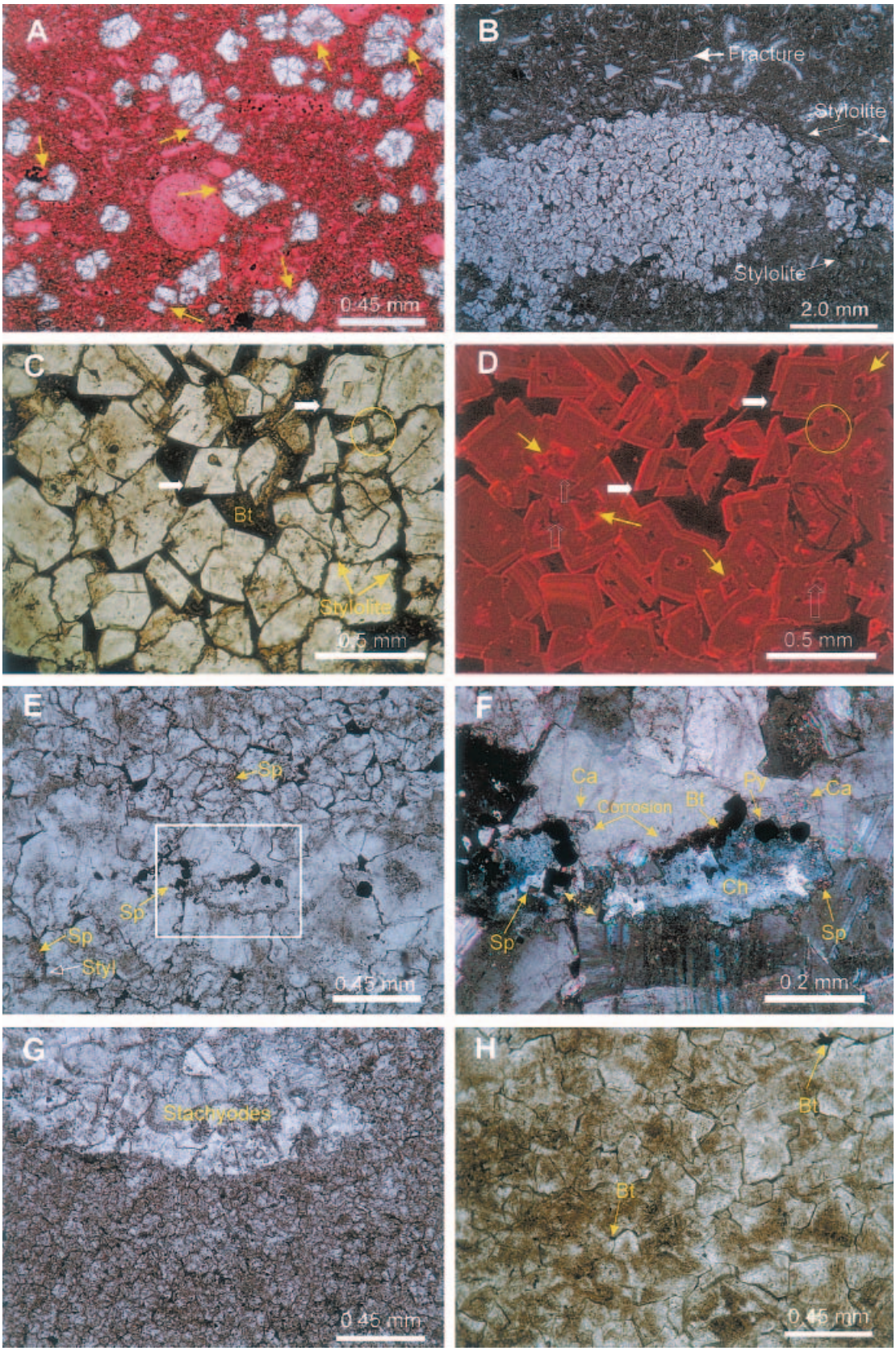
A
0.45 mm
B
Fracture
Stylolite
Stylolite
2.0 mm
C
Bt
Stylolite
0.5 mm
D
0.5 mm
E
Sp
Sp
Sp
Styl
0.45 mm
F
Ca
Corrosion
Bt
Py
Ca
Ch
Sp
Sp
0.2 mm
G
Stachyodes
0.45 mm
H
Bt
Bt
0.45 mm

Fig. 7. Replacement dolomites. (A) Photomicrograph of Rd1 dolomites, planar euhedral to subhedral crystals or cryptocrystals floating in the matrix of bioclastic wackestones (red stained with Alizarin Red-S). Note relatively large crystals with embayed or stepped surfaces (arrows). (B) Photomicrograph of Rd2 dolomites, planar-s (e) subhedral dolomite patches occurring along stylolites. (C and D) Paired photomicrographs of Rd2 dolomite mosaics under plane-polarized light and CL, which predate high-amplitude stylolites accompanying pressure corrosion (arrows in C). Locally, the stylolite cuts the dolomite crystal (see circled areas in C and D). Intercrystalline porosity is occluded by bitumen (Bt). Oscillatory luminescent zonation is apparent in crystals within which irregular (truncation) contacts between cores and out rims are present (arrows in D) in some crystals. Some crystals display similar shape to Cd2 dolomites (white arrows in C and D) and are completely truncated by the irregular cores (hollow arrows in D). (E) Photomicrograph of transitional dolomite textures between Rd2 and Rd3, subhedral to anhedral packed crystals with less porosity occluded by bitumen. Irregular dissolution seams are extensive between crystals and are disseminated with bitumen, pyrite and/or sphalerite (Sp) (amber brown, arrows), along which pressure corrosion and silicification also occurred. Note the stylolite (Styl), which cuts crystal grains locally (hollow arrow). The coarser crystal mosaic is probably a skeletal mould. (F) Details of inset box in (E). Serrated dissolution sutures disseminated with bitumen (Bt), pyrite (Py) (or sphalerite, Sp), followed by silicification (chert, Ch), corrosion (embayed surfaces) and calcitization (Ca). Chert replaced pyrite locally (dashed arrow). Crossed nichols. (G) Photomicrograph of Rd3 dolomites, medium, non-planar, anhedral crystals tightly packed with partly dolomitized skeletal *Stachyodes*. (H) Coarse-crystalline Rd3 dolomite mosaics, tightly packed, non-planar anhedral crystals with rare intercrystalline porosity occluded by bitumen (Bt, arrows).

Strontium isotopes

Twenty-six samples analysed for O–C isotopes were also assigned for Sr isotope analysis (Table 1; Fig. 11). The dolomitic limestones ($n = 2$) have the least radiogenic $^{87}Sr/^{86}Sr$ ratios from 0·7078 and 0·7084, close to the ratios of Middle Devonian sea water (0·7075–0·7080; cf. Burke *et al.*, 1982; Denison *et al.*, 1997). Two of the three Rd2 dolomites have intermediate $^{87}Sr/^{86}Sr$ ratios (0·7084–0·7088), but the third one is more radiogenic (0·7099). Most of the Rd3 dolomites ($n = 6$), including medium- and coarse-crystalline textures, have intermediate $^{87}Sr/^{86}Sr$ ratios from 0·7084 to 0·7090; two samples of Rd3 dolomites adjacent to Cd2 (saddle) dolomite cements, however, are highly radiogenic (0·7106 and 0·7114 respectively). Cd2 dolomite cements ($n = 6$) have the most radiogenic $^{87}Sr/^{86}Sr$ ratios ranging from 0·7098 to 0·7114, except for one less radiogenic sample (0·7086).

Stage 1 calcite cements have variable $^{87}Sr/^{86}Sr$ ratios from 0·7079 to 0·7096 (average 0·7087, $n = 6$), which are generally less radiogenic than those of Cd2 (saddle) dolomite cements (Fig. 11). Only one sample of Stage 2 vein calcite (TJB4-c) is available for Sr isotopic analyses, which yields a $^{87}Sr/^{86}Sr$ ratio of 0·7099, higher than that of Stage 1 calcite (Fig. 11).

FLUID INCLUSIONS

Two-phase (liquid–vapour) primary aqueous fluid inclusion assemblages (FIA) were observed along growth zones of the coarse-crystalline Rd3 dolomite, Cd2 saddle dolomite cement and Stage 1 calcite cement. Fluid inclusions in the dolomite are very small in size (3–8 μm), whereas those in the Stage 1 calcite are larger (6–30 μm). All these inclusions are irregular to elongate in shape. Each FIA has relatively consistent T_h and T_m values, suggesting a minimum effect of re-equilibration on T_h and T_m values.

Coarse-crystalline Rd3 dolomites have T_h values of 136–149 °C (average 145 °C) and T_m values of −7·6 to −4·5 °C (average −6·8 °C) (Table 2; Fig. 12A). Salinities, estimated from T_m values, vary from 7·2 and 11·2 wt% NaCl equivalent (Table 2; Fig. 12C). The Cd2 saddle dolomite in vugs yields T_h values from 175 to 209 °C (average 190 °C) and T_m values from −6·6 to −3·8 °C (average −5·1 °C) (Table 2; Fig. 12A). Calculated salinities vary from 6·2 to 10·0 wt% NaCl equivalent (average 8%) (Fig. 12C). The Cd2 saddle dolomite from veins has T_h values from 171 to 191 °C (average 185 °C), T_m values from −3·1 to −0·2 °C (average −1·7 °C) and salinities from 0·4 to 5·1 wt% NaCl equivalent (average 2·8%) (Table 2; Fig. 12A and C). The T_h values measured from vuggy calcite cements of Stage 1 range from 145 to 170 °C (average 159 °C) (Table 2; Fig. 12B), which are lower than those of Cd2 saddle dolomite cements, but higher than those of Rd3 replacement dolomites. In contrast, their T_m values are consistently high, from −0·1 to 0 °C, corresponding to very low salinities, from 0 to 0·2 wt% NaCl equivalent (Fig. 12C). No fluid inclusion data for calcite cements from Stage 2 are available in this study.

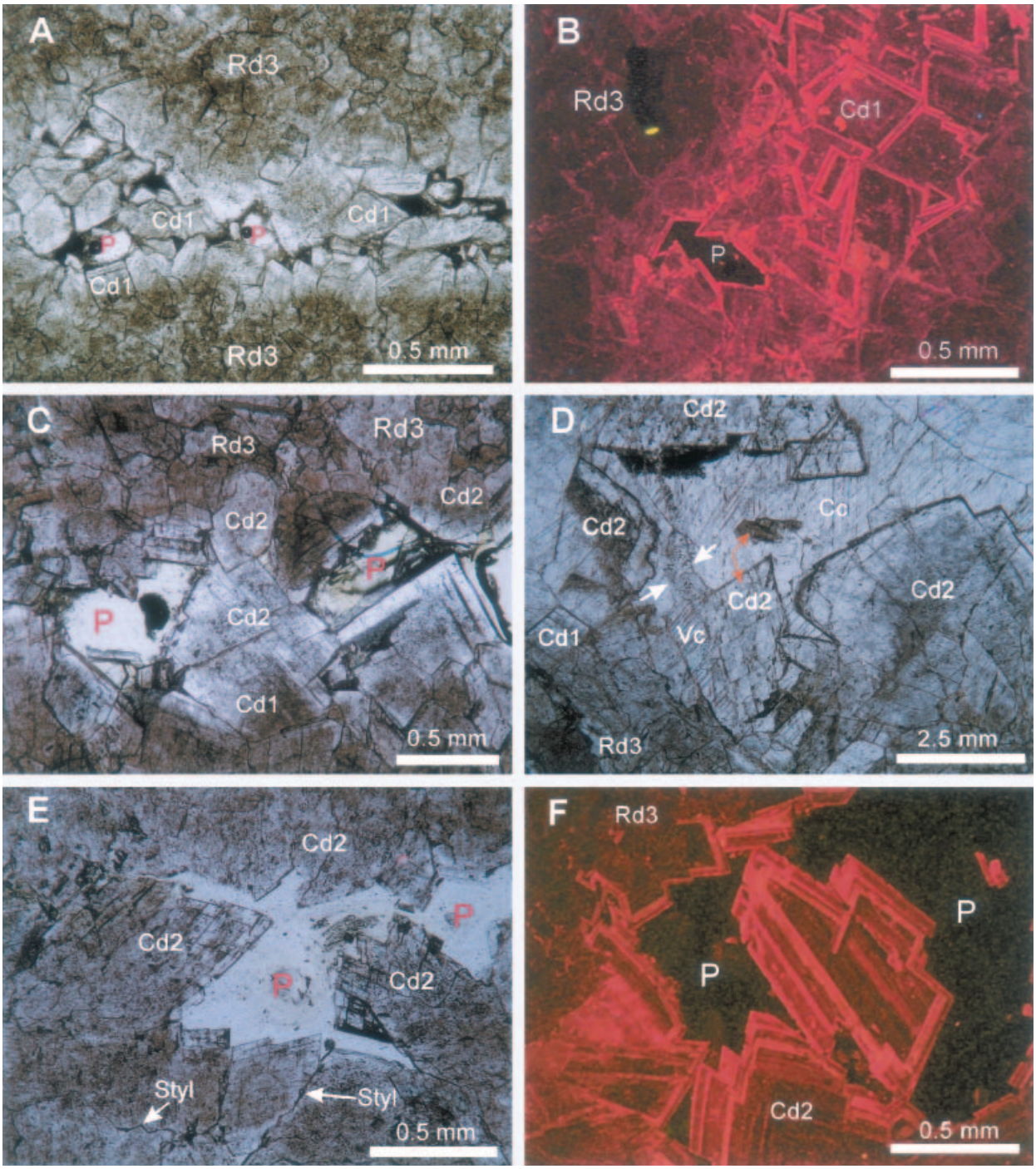

Fig. 8. Dolomite cements. (A) Photomicrograph of Cd1 cements, which line a mouldic vug in the Rd3 dolomite, under plane-polarized light. Note the remnant porosity (P) in the vuggy centre. (B) Cd1 cements lining a mouldic vug under CL. Dolomite crystals exhibit very dull blotchy luminescent thick cores with bright thin rims. Rd3 dolomites adjacent to the vug also show dull blotchy luminescence with thin rims under CL, suggesting later neomorphism. P, relict porosity. (C) Cd2 dolomite cements grow over Cd1 cements locally, both lining a mouldic vug in the Rd3 dolomite host with relict pores (P); the black fills in pores are contamination during thin-section preparation. (D) Photomicrograph showing the paragenetic sequence from Rd3 to Cd1 and Cd2 dolomites, then to vug-filling coarse calcite (Cc) and, finally, vein (or fracture) calcite (Vc, white arrows), which cross-cuts all previous mineral phases. Note the Cd2 breccia (orange arrow) within the coarse calcite (Cc). (E) Photomicrograph of Cd2 dolomite cements lining the mouldic vug in Rd3 dolomite host under plane-polarized light. Relict porosity (P) is present towards the centre. Stylolites occur until the termination of Cd2 dolomites (Styl). (F) Features of Cd2 dolomites under CL. Scimitar-like crystals exhibit very dull blotchy luminescent cores and bright red thin rims. P, relict porosity.

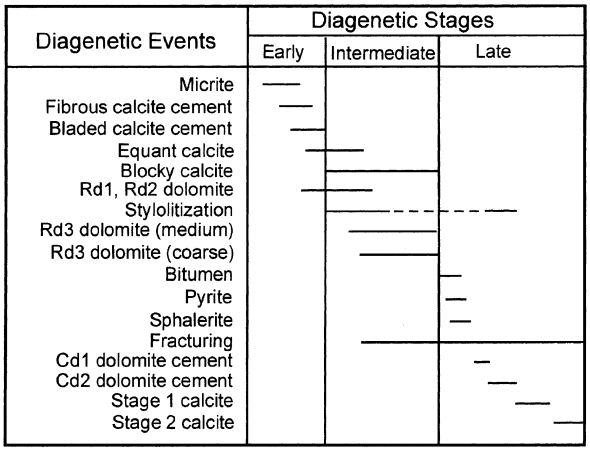

Fig. 9. Paragenetic sequence of Givetian carbonates (Tangjiawan Formation and the lower member of the Guilin Formation) in the study area. The early, intermediate and late stages are defined relative to stylolite formation. Stage 1 calcite includes vuggy calcite and early vein calcite (trending NW–SE); Stage 2 calcite only includes the late vein calcite (trending NE–SW).

DISCUSSION

Origin of replacement dolomite

Replacement dolomites occur extensively in the Givetian carbonates in both platformal and basinal facies, particularly in the basal Tangjiawan Formation (Figs 2, 4 and 5). Preferential dolomitization in more porous subtidal stromatoporoid buildups (Fig. 6A and B) and relatively weak dolomitization in peritidal facies, coupled with the upward decrease in abundance of dolomite from both platformal and basinal successions (Figs 4 and 5), suggests that dolomitization was independent of short- to long-term sea-level falls. This argues against mixing zone dolomitization being related to subaerial exposure as a possible mechanism for dolomitization in these Devonian carbonate rocks, as has been proposed by some authors (e.g. Shen *et al.*, 1994; Du *et al.*, 1996; Gong *et al.*, 1997).

The association of Rd1 and Rd2 dolomite rhombs/patches with low-amplitude stylolites (Fig. 7A and B) suggests dolomitization in a shallow burial environment (≈ 500 m; cf. Lind, 1993), approximately during the Early Frasnian (Fig. 3). Using a surface temperature of 25–30 °C and a normal geothermal gradient of 30 °C km^{-1} (cf. Qing & Mountjoy, 1989; Drivet & Mountjoy, 1997), this could only yield a burial temperature of 40–50 °C. The low $\delta^{18}O$ values of Rd2 dolomites (−10·9 to −10·3‰ VPDB) (Fig. 10), however, point to a higher temperature during dolomitization or a highly ^{18}O-depleted dolomitizing fluid (e.g. influx of meteoric waters). The stratigraphic and petrographic evidence, as stated earlier, does not support a freshwater influx during dolomitization. Moreover, the slightly higher $^{87}Sr/^{86}Sr$ ratios of the Rd2 dolomites (Fig. 11) than those of Middle Devonian sea water (Burke *et al.*, 1982; Denison *et al.*, 1997) suggest that the dolomitizing fluids may have been derived from connate

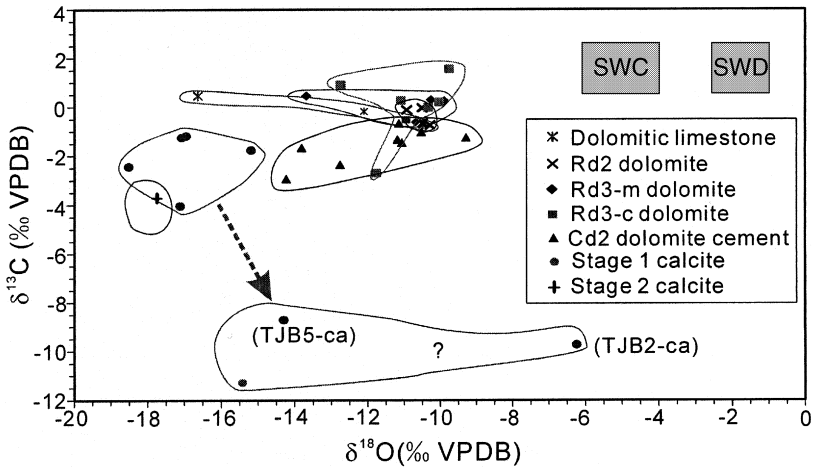

Fig. 10. Cross-plot of $\delta^{13}C$ and $\delta^{18}O$ values for dolomitic limestones, replacement dolomites (Rd2, Rd3), dolomite cements (Cd2) and late coarse calcite cements (Stage 1 and 2). The isotopic values of dolomitic limestones and replacement dolomites are highly mixed and overlap with those of Cd2 (saddle) dolomite cements, probably reflecting neomorphic alterations. Arrows represent the possible pathway of diagenetic fluid evolution for the calcite cements of Stage 1. Original isotopic values for sea-water calcite (SWC) and dolomite (SWD), based on Popp *et al.* (1986) and Qing & Mountjoy (1994), are given for reference. Rd3-m (or c), medium (or coarse)-crystalline Rd3 dolomites.

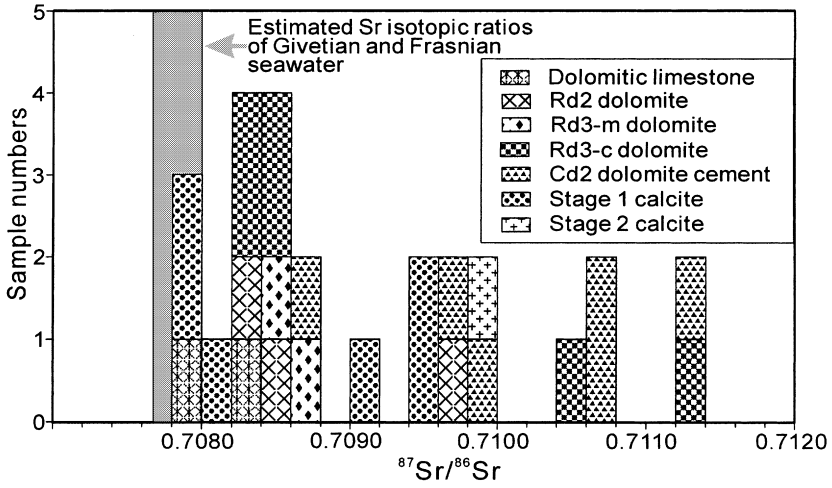

Fig. 11. Histogram showing variations in $^{87}Sr/^{86}Sr$ ratios for dolomitic limestones, replacement dolomites, dolomite cements and late calcite cements. Note the overlaps between different mineral phases. Coeval $^{87}Sr/^{86}Sr$ ratios of Givetian to Frasnian sea water for reference (0·7075–0·7080; Denison *et al.*, 1997). Rd3-m (or c) as in Fig. 10.

Table 2. Fluid inclusion data of Rd3, Cd2 dolomites and later calcite cements in the Givetian carbonates.

Sample	Mineral type	FIA	No. of inclusions	T_h (°C)			T_m (°C)			Salinity (wt% NaCl eq.)		
				Min.	Max.	Mean	Min.	Max.	Mean	Min.	Max.	Mean
TJB5	Vuggy calcite	1	4	149	156	154	−0·1	0·0	0·0	0·0	0·2	0·0
		2	5	153	170	163	−0·1	0·0	−0·1	0·0	0·1	0·1
		3	5	165	167	166	0·0	0·0	0·0	0·0	0·0	0·0
		4	5	152	165	158	−0·1	0·0	−0·1	0·0	0·2	0·1
		5	2	145	153	149	0·0	0·0	0·0	0·0	0·0	0·0
FHD-5	Vuggy Cd2 dolomite	1	9	175	209	193	−6·6	−4·0	−5·5	6·4	10·0	8·5
		2	5	182	187	185	−4·2	−3·8	−4·0	6·2	6·7	6·5
FHD-1	Rd3-c dolomite	1	6	136	149	145	−7·6	−4·5	−6·8	7·2	11·2	10·1
	Vein Cd2 dolomite	1	7	171	191	185	−3·1	−0·2	−1·7	0·4	5·1	2·8

sea water mixed with Frasnian sea water at elevated temperatures. Thus, a potential source of Sr, and perhaps Mg, for initial dolomitization may have been the Devonian sea water that was partially modified by rock–water interactions at elevated temperatures. Coincidently, widespread hydrothermal activities occurred from the latest Givetian to middle Famennian (e.g. Chen & Gao, 1988; Han & Hutchinson, 1990; Zhou, 1990; Chen *et al.*, 1998; Chen *et al.*, 2001a, 2002), as demonstrated by widespread basinal deposits of bedded chert interbedded with tuffaceous beds (or pillow lava in south-western Guangxi) in South China (e.g. Wu *et al.*, 1987; Jin, 1990). These hydrothermal activities could have greatly elevated the geothermal gradient and initiated dolomitization at burial depths of several hundred metres (Fig. 13A). During this period of shallow burial, sea water may also have reached the basal carbonates through syndepositional fault systems (Fig. 13A). Thus, the dolomite that formed at this time commonly had the imprints of sea-water signatures, as documented above. However, the high heat flow in the region could have eventually inhibited the formation of early replacement (planar) dolomites (Rd1, Rd2) in view of the kinetics of crystal growth (cf. Gregg & Sibley, 1984). On the other hand, it could also have accelerated the formation of pervasive Rd3 (non-planar) replacement dolomites.

Compared with Rd2 dolomites, the Rd3 dolomites consist of larger dolomite crystals with increasing non-planar crystal boundaries (Fig. 7H) and lower $\delta^{18}O$ values (−13·7 to −9·7‰ VPDB, average −11·0‰) (Fig. 10), suggesting that Rd3 dolomite formed at higher temperatures (cf. Gregg & Sibley, 1984; Gregg & Shelton, 1990; Montañez & Read, 1992). The T_h values of Rd3 dolomites range from 136 to 149 °C, much higher than the temperature created by the normal geothermal gradient (see later discussion). T_m values range from −7·6 to −4·5 °C (7·2–11·2 wt%

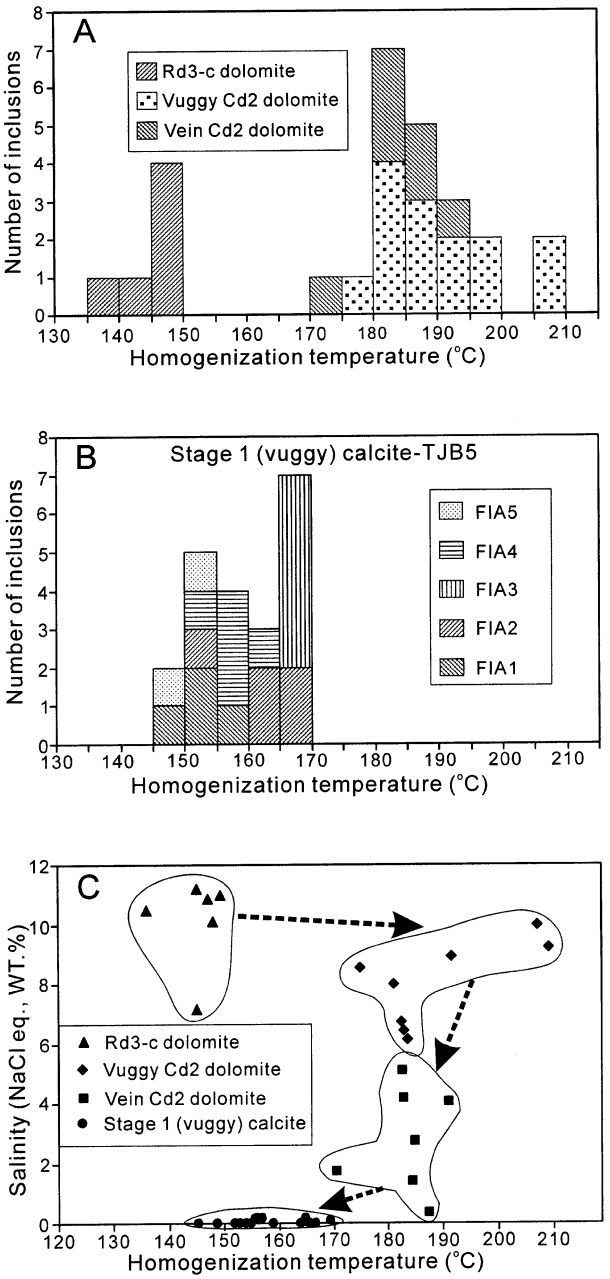

Fig. 12. (A) Homogenization temperatures of fluid inclusions in replacement dolomites (Rd3) and dolomite cements (Cd2). (B) Homogenization temperatures of vuggy calcite cements (TJB5; see Fig. 6). (C) Crossplot of salinity, calculated from final melting temperatures (T_m) of fluid inclusions, vs. homogenization temperatures (T_h) from fluid inclusions in replacement dolomites (Rd3), dolomite cements (Cd2) and vuggy calcite cements. Arrows represent possible pathway of fluid evolution.

NaCl equivalent) (Fig. 12A and C), indicating a hydrothermal, saline fluid from which the Rd3 dolomite precipitated (cf. Machel & Lonnee, 2002). The intermediate to high $^{87}Sr/^{86}Sr$ ratios of Rd3 dolomites (0·7084–0·7090 mostly; Fig. 11) also attest to an increased influence of saline basinal fluids (Fig. 13B), probably sourced from buried siliciclastics that were enriched in ^{87}Sr and Mg^+ as a result of extensive silicate diagenesis and compaction (Stueber *et al.*, 1984; Gao & Land, 1991; Banner, 1995).

The partial overlap of $\delta^{18}O$ values of Rd3 dolomites with those of Rd2 dolomites may also reflect an overlap of timing in their formation and/or neomorphism upon Rd2 dolomites (see later discussion), so that Rd3 dolomites may have originated intermittently through hydrothermal anomalies from the Late Devonian to Early Carboniferous at burial depths of 1·5–2·5 km (Fig. 3). This was much shallower than the burial depths (3·5–4 km) calculated using T_h values of Rd3 dolomites (136–149 °C) and a normal geothermal gradient. The high heat flow could have heated up the fluids that had already circulated downwards to the deeply buried sediments and driven them to migrate upwards preferentially along fault/fracture systems (e.g. Tsang & Neretnieks, 1998; Fisher & Becker, 2000) into the porous basal biostromal facies, leading to pervasive dolomitization along these fluid conduit systems (Fig. 13B). However, the amount of Mg in the fluids would have been reduced significantly as a result of dolomitization. So, when these fluids continued to migrate upwards into the carbonate horizons above the Givetian strata, dolomitization was mainly localized along the fault zones.

Origin of dolomite cement

Two types of dolomite cements are recognized in this study: planar-e (s) (Cd1) and non-planar saddle dolomite (Cd2). The brecciation of host dolostones before the dolomite cements (Fig. 6B and D) suggests an overpressure hydrofracturing (e.g. Fontboté & Gorzawski, 1990; Nielsen *et al.*, 1998) in response to huge lithostatic loads or tectonic compression, as a result of basin inversion during the Early Triassic (at burial depths of 5·5–7 km; Fig. 3). Moreover, the presence of dolomite cements without secondary corrosion in open vugs (Figs 6B and 8A–C and E–F) excludes the possibility of dissolution as a cause for the voids; on the other hand, it suggests that dolomitization might have occurred under a pore fluid pressure high enough to sustain the pore spaces in the context of high lithostatic pressures (Nielsen *et al.*, 1998; Boni *et al.*, 2000). This further constrains the timing of precipitation of dolomite cements to being before a significant uplift (or exhumation) of the basin.

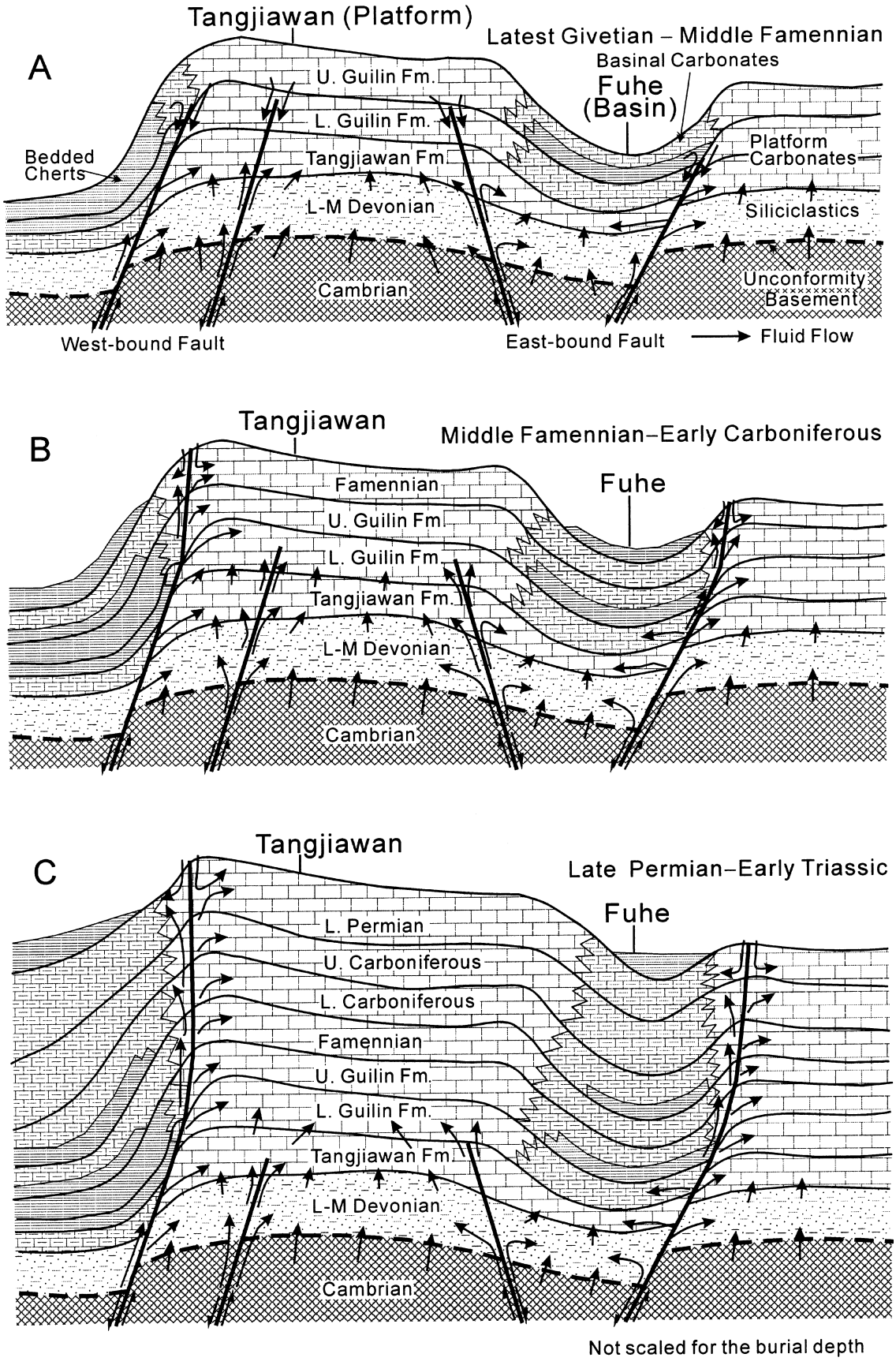
A
Tangjiawan (Platform)
Latest Givetian – Middle Famennian
Basinal Carbonates
Fuhe
(Basin)
U. Guilin Fm.
L. Guilin Fm.
Tangjiawan Fm.
L-M Devonian
Cambrian
Bedded
Cherts
Platform
Carbonates
Siliciclastics
Unconformity
Basement
West-bound Fault
East-bound Fault
Fluid Flow
B
Tangjiawan
Middle Famennian–Early Carboniferous
Fuhe
Famennian
U. Guilin Fm.
L. Guilin Fm.
Tangjiawan Fm.
L-M Devonian
Cambrian
C
Tangjiawan
Late Permian–Early Triassic
Fuhe
L. Permian
U. Carboniferous
L. Carboniferous
Famennian
U. Guilin Fm.
L. Guilin Fm.
Tangjiawan Fm.
L-M Devonian
Cambrian
Not scaled for the burial depth

Fig. 13. Conceptual model of dolomitization in the Guilin area. Faults (syndepositional or reactivated) played a critical role in channelling fluids into the porous basal biostromal (or reefal) facies of the Devonian during several hydrothermal anomalies in the context of increasing burial. (A) The basal Givetian carbonates (Tangjiawan Fm. and Lower Member of Guilin Fm.) were subjected to the first strong hydrothermal anomaly from the latest Givetian to middle Famennian times when they were buried at shallow depth (≈ 400–600 m). High heat flow with involvement of (connate or downflow) sea water led to initial dolomitization. (B) The basal carbonates were subjected to the second hydrothermal anomaly during intermediate to deep burial, mostly within the Early Carboniferous. Fluids that mainly originated in deep-seated basins were channelled along reactivated faults/fractures and migrated upwards to the basal carbonates, leading to intense pervasive dolomitization. The overlying carbonate strata subjected to weak dolomitization would be more resistant to later dolomitizing fluids except for the strata adjacent to faults. (C) The basal carbonates experienced later hydrothermal anomalies mainly from the Late Permian to the Early Triassic in the context of deeper burial (see Fig. 3).

Cd2 saddle dolomite cements yield the lowest $\delta^{18}O$ values (−14·2 to −9·3‰ VPDB), the highest T_h values (170–209 °C) and the most radiogenic $^{87}Sr/^{86}Sr$ ratios (≈ 0·7100) (Figs 10, 11 and 12A), similar to those reported elsewhere around the world (cf. Kaufman *et al.*, 1991; Mountjoy & Halim-Dihardja, 1991; Qing & Mountjoy, 1992, 1994). At a normal geothermal gradient of 30 °C km^{-1} with a surface temperature of 25–30 °C (see earlier discussion), a burial depth of 5–7 km (Fig. 3) could yield a burial temperature of 180–240 °C, similar to fluid inclusion T_h values. However, the measured T_h values only represent the minimum temperature at which the fluid inclusions were trapped (Goldstein & Reynolds, 1994); the real trapping temperatures (T_r) with pressure correction at which the Cd2 dolomite precipitated could be much higher than the T_h values. Assuming that fluid inclusions were trapped under lithostatic pressure with an average rock density of 2·65 g cm^{-3} (cf. Asquith, 1982) at a burial depth of 5–7 km, pressure corrections were made from the intersection of trapping pressure (i.e. lithostatic pressure) and established isochores for measured fluid inclusions using the FLINCOR program (Brown, 1989). As a result, true T_r values were 260–270 °C at a burial depth of 5 km, about 80–90 °C higher than the normal burial temperature. At the burial depth of 7 km, T_r values were 290–300 °C, about 50–60 °C higher than the normal burial temperature.

These data therefore suggest that the saddle dolomites precipitated at abnormally high temperatures from hydrothermal fluids (cf. Machel & Lonnee, 2002), most probably sourced from the underlying siliciclastics or deeper seated Cambrian basement. During the deep burial of the host carbonates, there were extensive hydrothermal activities, as documented earlier (Sha *et al.*, 1990; Liu *et al.*, 1993; Wang *et al.*, 1994). The heat flow anomalies would drive the fluids that originated in the underlying deep-buried siliciclastics to migrate preferentially along the flow pathways established during earlier dolomitization (e.g. Duggan *et al.*, 2001; Gregg *et al.*, 2001), leading to more intense dolomitization (Fig. 13C). These fluids could have also resulted in neomorphism of precursor dolomites (see later discussion), dissolution of calcitic allochems and development of moulds and vugs in replacement dolomite (Figs 6B and C and 8).

Dolomite cements precipitated mostly from fluids more saline than sea water (mostly >4 wt% NaCl equivalent; Table 2; Fig. 12C). However, the relatively low $^{87}Sr/^{86}Sr$ ratio (0·7086) and salinity values (0·4–5·1 wt% NaCl equivalent) of some vein Cd2 dolomite cements (e.g. FHD1-s) (Tables 1 and 2; Figs 11 and 12C) suggest that they may have precipitated after invasion of freshwater into the host Devonian carbonate strata (cf. Assereto & Folk, 1980; Gao & Land, 1991), as the basin initiated uplift from the early Middle Triassic. Progressive recharge of meteoric fluids into the carbonate host rocks as a result of further uplift of the basin, however, finally ended the dolomitization as the fluids became undersaturated with respect to dolomite and switched to calcitization (see later discussion).

Dolomite neomorphism

Neomorphism (or recrystallization) of earlier formed dolomites is a common process during progressive burial of dolomites (Land, 1985; Kaufman *et al.*, 1991; Mazzullo, 1992; Nielsen *et al.*, 1994; Drivet & Mountjoy, 1997; Durocher & Al-Aasm, 1997; Al-Aasm & Packard, 2000). In this study, the increase in crystal size from Rd1 to Rd2 dolomites concomitant with an increase in nonplanar crystal boundaries (Fig. 7A–F) implies that their formation was involved with later higher temperature, dolomitizing fluids (e.g. Sibley & Gregg, 1987; Montañez & Read, 1992). The occurrence of petal-like or irregular dark cores of some Rd2 dolomites (Fig. 7B, E and F) is likely to be a result of neomorphic modifications caused

by fluids responsible for Rd3 dolomites. Similar crystal shape of some Rd2 dolomites to Cd2 dolomites (Fig. 7C and D) suggests an alteration of Rd2 dolomites during the precipitation of Cd2 dolomites. Irregular (truncation) contacts between cores and outer overgrowths in Rd2 dolomites (Fig. 7D) suggest partial dissolution of early dolomite cores by later dolomitizing fluids and reprecipitation (e.g. Nielsen *et al.*, 1994; Durocher & Al-Aasm, 1997). Furthermore, similar CL patterns of Rd3 dolomites to adjacent dolomite cements (Fig. 8B and F) also point towards an alteration of the former dolomites, caused by the fluids responsible for later dolomite cements (e.g. Kaufman *et al.*, 1991).

The large overlaps of $\delta^{18}O$ values between different types of replacement dolomites (Fig. 10) suggest that the early formed dolomites (Rd1 and Rd2) were neomorphosed by later dolomitizing fluids (i.e. for Rd3 dolomites). Similarly, overlaps of $\delta^{18}O$ values and $^{87}Sr/^{86}Sr$ ratios between Cd2 dolomite cements and some replacement dolomites (Figs 10 and 11) also suggest neomorphism of the replacement dolomites when they were exposed to the later hydrothermal fluids responsible for the precipitation of Cd2 dolomites.

Late-stage calcite cement

The late-stage, coarse to very coarse calcite postdates all the dolomites and occurs as cements in fractures and vugs. The brecciation of Cd2 dolomites before precipitation of vuggy calcite cements (Fig. 8D) may reflect a tectonic compression in response to the initial Indosinian Orogeny. As documented earlier, the void- and vein-filling calcite cements were formed in two phases (Figs 6E and 8D). Furthermore, the coincidence in orientation of NE- to SW-trending, calcite-filled (Stage 2) fractures/veins with the principal structural domain, formed during the late Indosinian from Late Triassic (Han & Yang, 1980; GMRBG, 1988, 1994), strongly suggests their genetic relationship with this orogenic episode. Under this circumstance, calcite cements of Stage 1, including vuggy calcite and NW- to SE-trending vein calcite, are reasonably constrained to have formed in response to basin uplift during the early Indosinian Orogeny.

The high T_h values (145–170 °C) and low salinities (≈ 0·0 wt% NaCl equivalent) of fluid inclusions of Stage 1 vuggy calcite cements (Table 2; Fig. 12B and C) suggest that they precipitated from highly dilute (meteoric) fluids at high temperatures. The increase in $\delta^{18}O$ values with corresponding decrease in $\delta^{13}C$ values (Fig. 10) probably reflects a cooling fluid with increased influences of organic carbon. The termination of hydrocarbon migration before the precipitation of dolomite cements (Cd1 and Cd2) (see earlier documentation) excludes the possibility of hydrocarbon involvement. These variations agree well with the uplift of the host carbonate rocks from deep burial (≈ 5000–7000 m) to exhumed basin (Fig. 3) during the course of the Indosinian Orogeny (early Middle Triassic). Under this circumstance, higher temperature fluids, with less CO_2 contribution from soil zone processes during the deep burial, reasonably reconcile the relatively high $\delta^{13}C$ and the lowest $\delta^{18}O$ values of the calcite cements. Accordingly, during the course of uplift of the basin, gradually cooling fluids, with increased CO_2 derived from soil zone processes through respiration of plant roots and oxidation of dead plant material (cf. Muchez *et al.*, 1998), account for the decreased $\delta^{13}C$ and increased $\delta^{18}O$ values of the calcite (Fig. 10). An increase in $^{87}Sr/^{86}Sr$ ratios with increased $\delta^{18}O$ values (except for TJB2-c; Figs 10 and 11) may have resulted from increased influxes of Sr from terrigenous material during uplift of the basin.

One Stage 2 calcite sample yields an intermediate low $\delta^{13}C$ value (−3·7‰ VPDB), a very low $\delta^{18}O$ value (−17·7‰ VPDB) and a radiogenic $^{87}Sr/^{86}Sr$ ratio (0·7099) (Figs 10 and 11), suggesting that some Stage 2 calcite cements might have precipitated from high-temperature (meteoric?) fluids originating from deep-buried siliciclastic deposits, with a minor contribution of CO_2 derived from soil zone processes. The recurrent subsidence that started from the Late Triassic (Fig. 3), as demonstrated by the Late Triassic continental lake deposits in the study area (GMRBG, 1988, 1994), may reconcile the scenario stated above. However, it is hard to constrain the fluid flow event for Stage 2 calcite cements in the absence of additional evidence from fluid inclusions and isotopic data.

CONCLUSIONS

Massive Devonian dolostones in the Guilin area are restricted to the basal (Givetian) strata that overlie thick (> 1000 m) siliciclastics of the Lower and Middle Devonian; they occur preferentially in stromatoporoid biostromal (or reefal) facies and decrease sharply in abundance in the

overlying carbonates. Three types of replacement dolomites were identified: fine-crystalline, planar-e (s), floating dolomite rhombs (Rd1); medium- to coarse-crystalline, planar-s (e), patchy/mosaic dolomites (Rd2); and medium- to very coarse-crystalline, non-planar, mosaic dolomites (Rd3). Minor dolomite cements include planar-e (Cd1) and non-planar (saddle) dolomites (Cd2), precipitated in moulds, vugs and fractures. Locally, late-stage coarse to very coarse calcite cements occur in vugs and fractures (or veins). Based on several lines of evidence from $\delta^{13}C$ and $\delta^{18}O$ values, $^{87}Sr/^{86}Sr$ ratios and fluid inclusion data, replacement dolomites could have formed in fluids from modified Devonian sea waters or hydrothermal, saline fluids from underlying siliciclastic successions, which provided the necessary ^{87}Sr and Mg^{+} material; dolomite cements precipitated from higher temperature, hydrothermal fluids probably derived from deeper buried siliciclastic sediments. These hydrothermal fluids could also have resulted in neomorphism of earlier formed dolomites. However, the invasion of meteoric water during the late stage of dolomitization as a result of basin uplift during the course of the Indosinian Orogeny finally stopped the dolomitization, leading to the precipitation of late-stage calcite cements. The systematic variations in $\delta^{13}C$ and $\delta^{18}O$ values, $^{87}Sr/^{86}Sr$ ratios and fluid inclusion data from later calcite cements further suggest the basin exhumation and associated soil zone processes in response to the Indosinian Orogeny.

Hydrothermal activities provided heat sources for the dolomitization, and four major hydrothermal events occurred during the late Givetian–middle Famennian, Early Carboniferous and Permian–Triassic. Faulting created important fluid conduits through which the sea water may have moved downwards to the basal carbonates at shallow depth or through which deep-origin hydrothermal fluids were driven upwards to the host rocks, leading to more intense dolomitization (i.e. R3, Cd1 and Cd2) at greater depth.

ACKNOWLEDGEMENTS

This work was supported by the National Natural Science Foundation of China (grant nos 49872043 and 40372062). H. Qing's work was supported by NSERC Discovery Grant 11052. We thank senior geologist Bao'an Yin of the Regional Geological Survey and Research of Guangxi, who provided invaluable help during several field seasons. Thanks also go to Dr Tim Prokopiuk at the Isotope Laboratory of the University of Saskatchewan, who helped to perform the isotope analysis. Part of the work was carried out when the senior author stayed at the University of Regina as a postdoctoral fellow. Constructive criticisms from K. Shelton, R. Swennen and editorial comments from C. Spötl greatly improved the manuscript.

REFERENCES

Al-Aasm, I.S. and **Packard, J.J.** (2000) Stabilization of early-formed dolomite: a tale of divergence from two Mississippian dolomites. *Sed. Geol.*, **131,** 97–108.

Amthor, J.E., Mountjoy, E.W. and **Machel, H.** (1993) Subsurface dolomites in Upper Devonian Leduc Formation buildups, central part of Rimbey-Meadowbrook reef trend, Alberta, Canada. *Bull. Can. Petrol. Geol.*, **41,** 164–185.

Asquith, G.B. (1982) *Basic Well Log Analysis for Geologists.* AAPG Methods in Exploration Series, **3,** 216 pp.

Assereto, R. and **Folk, R.L.** (1980) Diagenesis fabrics of aragonite, calcite, and dolomite in an ancient peritidal-spelean environment: Triassic Calcare Rosso, Lombardia, Italy. *J. Sed. Petrol.*, **50,** 371–394.

Banner, J.L. (1995) Application of the trace element and isotope geochemistry of strontium to studies of carbonate diagenesis. *Sedimentology*, **42,** 805–824.

Bodnar, R.J. (1993) Revised equation and table for determining the freezing point depression of H_2O–NaCl solutions. *Geochim. Cosmochim. Acta*, **57,** 683–684.

Boni, M., Parente, G., Bechstädt, T., De Vivo, B. and **Iannace, A.** (2000) Hydrothermal dolomites in SW Sardinia (Italy): evidence for a widespread late-Variscan fluid flow event. *Sed. Geol.*, **131,** 181–200.

Braithwaite, C.J.R. and **Rizzi, G.** (1997) The geometry and petrogenesis of hydrothermal dolomites at Navan, Ireland. *Sedimentology*, **44,** 421–440.

Brown, P.E. (1989) FLINCOR: a microcomputer program for the reduction and investigation of fluid inclusion data. *Am. Mineral.*, **74,** 1390–1393.

Burke, W.H., Denison, R.E., Hetherington, E.A., Koepnick, R.B., Nelson, H.F. and **Otto, J.B.** (1982) Variations of seawater $^{87}Sr/^{86}Sr$ throughout Phanerozoic time. *Geology*, **10,** 516–519.

Chen, D.Z., Tucker, M.E., Zhu, J.Q. and **Jiang, M.S.** (2001a) Carbonate sedimentation in a starved pull-apart basin, Middle to Late Devonian, southern Guilin, South China. *Basin Res.*, **13,** 141–167.

Chen, D.Z., Tucker, M.E., Jiang, M.S. and **Zhu, J.Q.** (2001b) Long-distance correlation between tectonic-controlled, isolated carbonate platforms by cyclostratigraphy and sequence stratigraphy in the Devonian of South China. *Sedimentology*, **48,** 57–78.

Chen, D.Z., Tucker, M.E., Zhu, J.Q. and **Jiang, M.S.** (2002) Carbonate platform evolution from a bioconstructed platform margin to a sand-shoal system (Devonian, Guilin, South China). *Sedimentology*, **49,** 737–764.

Chen, H.M., Wu, X.H., Zhang, Y., Li, Y.X., Wen, Q.Y., Fu, D.X., Yan, C.X., Liu, W.H., Chen, W.Y. and **Wang, D.P.** (1994) *Carboniferous Lithofacies, Palaeogeography and Mineralization in South China.* Geological Publishing House, Beijing, China, 123 pp.

Chen, X.M., Deng, J. and **Zhai, Y.S.** (1998) The physical and chemical environment of Fankou Pb-Zn deposits formed by submarine hot-spring. *Mineral Deposita*, **17,** 240–246 (in Chinese with English abstract).

Chen, X.P. and **Gao, J.Y.** (1988) Thermal water deposition and Pb-Zn barite deposits in the Devonian System, Central Guangxi. *Chin. J. Geochem.*, **7,** 321–328.

Denison, R.E., Koepnick, R.B., Burke, W.H., Hetherington, E.A. and **Fletcher, A.** (1997) Construction of the Silurian and Devonian seawater $^{87}Sr/^{86}Sr$ curve. *Chem. Geol.*, **140,** 109–121.

Dickson, J.A.D. (1965) A modified staining technique for carbonates in thin section. *Nature*, **205,** 587.

Doglioni, C. and **Goldhammer, R.K.** (1988) Compaction-induced subsidence in the margin of a carbonate platform. *Basin Res.*, **1,** 237–246.

Drivet, E. and **Mountjoy, E.W.** (1997) Dolomitization of the Leduc Formation (Upper Devonian), southern Rimbey-Meadowbrook reef trend, Alberta. *J. Sed. Res.*, **67,** 411–423.

Du, Y.S., Gong, Y.M. and **Wu, Y.** (1996) Devonian sequence stratigraphy and sea-level change cycles in South China. *J. China Univ. Geosci.*, **7,** 72–79.

Duggan, J.P., Mountjoy, E.W. and **Stasiuk, L.D.** (2001) Fault-controlled dolomitization at Swan Hills Simonette oil field (Devonian), deep basin west-central Alberta, Canada. *Sedimentology*, **48,** 301–323.

Durocher, S. and **Al-Aasm, I.S.** (1997) Dolomitization and neomorphism of Mississipian (Visean) Upper Debolt Formation, Blueberry Field, northeastern British Columbia: geologic, petrologic, and chemical evidence. *AAPG Bull.*, **81,** 954–977.

Feng, Z.Z., Bao, Z.D. and **Li, S.W.** (1997) *Lithofacies Palaeogeography of Middle and Lower Triassic of South China*. Petroleum Industry Press, Beijing, China, 222 pp.

Feng, Z.Z., Yang, Y.Q., Bao, Z.D., Jin, Z.K., Zhang, H.Q., Wu, X.H. and **Qi, D.L.** (1998) *Lithofacies Palaeogeography of the Carboniferous in South China*. Geological Publishing House, Beijing, China, 119 pp.

Fisher, A.T. and **Becker, K.** (2000) Channelized fluid flow in oceanic crust reconciles heat-flow and permeability data. *Nature*, **403,** 71–74.

Fontboté. L. and **Gorzawski, H.** (1990) Genesis of the Mississipian Valley-type Zn-Pb deposits of San Vincente, Central Peru: geological and isotopic (Sr, O, C, S, Pb) evidence. *Econ. Geol.*, **85,** 1402–1437.

Gao, G.Q. and **Land, L.S.** (1991) Early Ordovician Cool Creek dolomite, Middle Arbuckle Group, Slick Hills, SW Oklahoma, USA: origin and modification. *J. Sed. Petrol.*, **61,** 161–173.

GMRBG (Geology and Mineral Resource Bureau of Guangxi) (1988) *Report of Regional Geological Survey of Guilin city (scale: 1/50,000).* Irregular publication (in Chinese), 288 pp.

GMRBG (Geology and Mineral Resource Bureau of Guangxi) (1994) *Report of Regional Geological Survey of Guilin-Yangshuo area (scale: 1/50,000).* Irregular publication (in Chinese), 79 pp.

Goldhammer, R.K. (1997) Compaction and decompaction algorithms for sedimentary carbonates. *J. Sed. Res.*, **67,** 26–35.

Goldstein, R.H. and **Reynolds, T.J.** (1994) Systematics of fluid inclusions in diagenetic minerals. *SEPM Short Course*, **31,** 199 pp.

Gong, Y.M., Wu, Y., Du, Y.S., Feng, Q.L. and **Liu, B.P.** (1997) The Devonian sea-level change rhythms in South China and coupling relationships of the spheres of the Earth. *Acta Geol. Sinica*, **71,** 212–226 (in Chinese with English abstract).

Gou, H.C. (1985) Primary research on tectonic background and provenances of turbidite deposits of Middle–Upper Triassic in Yunnan, Guizhou and Guangxi Provinces. *Acta Sedimentol. Sinica*, **3–4,** 95–107.

Gregg, J.M. and **Shelton, K.L.** (1990) Dolomitization and dolomite neomorphism in the back reef facies of the Bonneterre and Davis Formation (Cambrian), southeastern Missouri. *J. Sed. Petrol.*, **60,** 549–562.

Gregg, J.M. and **Sibley, D.F.** (1984) Epigenetic dolomitization and the origin of xenotopic dolomite texture. *J. Sed. Petrol.*, **54,** 908–931.

Gregg, J.M., Shelton, K.L., Johnson, A.W., Somerville, I.D. and **Wright, W.R.** (2001) Dolomitization of the Waulsortian Limestone (Lower Carboniferous) in the Irish Midlands. *Sedimentology*, **48,** 745–766.

Han, D.X. and **Yang, Q.** (1980) *Coal Geology of China (Part II).* Coal Industry Press, Beijing, China, 415 pp.

Han, F. and **Hutchinson, R.W.** (1990) Evidence for exhalative origin of the Dachang tin-polymetallic sulfide deposits – their geological and geochemical characteristics. *Mineral Deposita*, **9,** 319–324 (in Chinese with English abstracts).

Jin, Y.J. (1990) The diachronism of the Dinghechong Formation (bedded chert). *J. Stratigr.*, **14,** 131–135 (in Chinese).

Kaufman, J., Hanson, G.N. and **Meyers, W.J.** (1991) Dolomitization of the Devonian Swan Hills Formation, Rosevear Field, Alberta, Canada. *Sedimentology*, **38,** 41–66.

Land, L.S. (1985) The origin of massive dolomite. *J. Geol. Educ.*, **33,** 112–125.

Lind, I. (1993) Stylolites in chalks from Leg 130, Ontong Java Plateau. In: *Proceedings of the Ocean Drilling Program Scientific Results* (Eds W.H. Berger, J.W. Kroenk, L.A. Mayer et al.), **130,** 445–451.

Liu, B.J., Xu, X.S., Pan, S.N., Huang, H.Q. and **Xu, Q.** (1993) *Sedimentary, Crustal Evolution and Mineralization of South China Palaeo-Contintent.* Science Press, Beijing, China, 236 pp.

Machel, H.G. and **Lonnee, J.** (2002) Hydrothermal dolomite – a product of poor definition and imagination. *Sed. Geol.*, **152,** 163–171.

Mazzullo, S.J. (1992) Geochemical and neomorphic alteration of dolomite: a review. *Carbonates Evaporites*, **7,** 21–37.

Montañez, I.P. and **Read, J.F.** (1992) Fluid–rock interaction during stabilization of early dolomites, Upper Knox Group (Lower Ordovician), US Appalachian. *J. Sed. Petrol.*, **62,** 753–778.

Mountjoy, E.W. and **Halim-Dihardja, M.K.** (1991) Multiple phase fracture and fault-controlled burial dolomitization, Upper Devonian Wabamun Group, Alberta. *J. Sed. Petrol.*, **61,** 590–612.

Muchez, P., Nielsen, P., Sintubin, M. and **Lagrou, D.** (1998) Conditions of meteoric calcite formation along a Variscan fault and their possible relation to climatic evolution during the Jurassic–Cretaceous. *Sedimentology*, **45,** 845–854.

Nielsen, P., Swennen, R. and **Keppens, E.** (1994) Multiple-step recrystallization within massive ancient dolomite units: an example from the Dinantian of Belgium. *Sedimentology*, **41,** 567–584.

Nielsen, P., Swennen, R., Muchez, P. and **Keppens, E.** (1998) Origin of Dinantian zebra dolomites south of the Brabant-Wales Massif, Belgium. *Sedimentology*, **45,** 727–743.

Popp, B.N., Anderson, T.F. and **Sandberg, P.A.** (1986) Textural, elemental and isotopic variations among constituents in Middle Devonian limestones, North America. *J. Sed. Petrol.*, **56,** 715–727.

Qing, H.R. and **Mountjoy, E.W.** (1989) Multistage dolomitization in Rainbow buildups, Middle Devonian Keg River Formation, Alberta, Canada. *J. Sed. Petrol.*, **59,** 114–126.

Qing, H.R. and **Mountjoy, E.W.** (1992) Large-scale fluid flow in the Middle Devonian Presqu'ile barrier, Western Canada Sedimentary Basin. *Geology*, **20,** 903–906.

Qing, H.R. and **Mountjoy, E.W.** (1994) Formation of coarsely crystalline, hydrothermal dolomite reservoirs in the Presqu'ile Barrier, Western Canada Sedimentary Basin. *AAPG Bull.*, **78,** 55–77.

Sha, Q.A., Wu, W.S. and **Fu, J.M.** (1990) *Comprehensive Research on Permian in Guizhou–Guangxi Area and its Petroleum Potential*. Science Press, Beijing, China, 215 pp with 37 plates.

Shen, D.Q., Chen, Y.Q. and **Yang, Z.Q.** (1987) *Sedimentary Facies, Palaeogeography and Their Controls Over Ore Deposits of the Qiziqiao Formation (Upper Middle Devonian), South China*. Geological Publishing House, Beijing, 135 pp.

Shen, J.W., Yu, C.M., Yin, B.A. and **Zhang, S.L.** (1994) Reef complexes and sequences of Devonian carbonate platforms in Guilin. *J. Stratigr.*, **18,** 161–166 (in Chinese with English abstract).

Sibley, D.F. and **Gregg, J.M.** (1987) Classification of dolomite rock textures. *J. Sed. Petrol.*, **57,** 967–975.

Stueber, A.M., Pushkar, P. and **Hetherington, E.A.** (1984) A strontium isotopic study of Smackover brines and associated solids, southern Arkansas. *Geochim. Cosmochim. Acta*, **47,** 687–695.

Tsang, C.F. and **Neretnieks, I.** (1998) Flow channelling in heterogeneous fractured rocks. *Rev. Geophys.*, **36,** 275–298.

Wang, H.Z. (1985) *Atlas of the Palaeogeography of China*. Cartographic Publishing House, Beijing, China.

Wang, L.T., Lu, Y.B., Zhao, S.J. and **Luo, J.H.** (1994) *Permian Lithofacies, Palaeogeography and Mineralization in South China*. Geological Publishing House, Beijing, China.

Wendte, J., Qing, H.R., Dravis, J.J., Moore, S.L.O., Stasiuk, L.D. and **Ward, D.** (1998) High-temperature saline (thermoflux) dolomitization of Devonian Swan Hills platform and bank carbonates, Wild River area, west-central Alberta. *Bull. Can. Petrol. Geol.*, **46,** 210–265.

Wilkinson, J.J. and **Earls, G.** (2000) A high-temperature hydrothermal origin for black dolomite matrix breccias in the Irish Zn-Pb orefield. *Mineral. Mag.*, **64,** 1017–1036.

Wu, Y., Zhou, F.L., Jiang, T.C., Fang, D.N. and **Huang, W.S.** (1987) *The Sedimentary Facies, Palaeogeography and Relative Mineral Deposits of the Devonian in Guangxi*. Guangxi People's Publishing House, Nanning, China, 292 pp.

Zeng, Y.F., Chen, H.D., Zhang, J.Q. and **Liu, W.J.** (1992) Types and main characteristics of Devonian sedimentary basins in South China. *Acta Sedimentol. Sinica*, **10,** 104–113 (in Chinese with English abstract).

Zhong, G., Wu, Y., Yin, B.A., Liang, Y.L., Yao, Z.G. and **Peng, G.L.** (1992) *Devonian of Guangxi*. China University of Geoscience Press, Wuhan, China, 384 pp with 18 plates.

Zhou, Y.Z. (1990) Geochemical features of hydrothermally-originated siliceous rocks in Danchi (Nadan-Hechi) Basin. *Acta Sedimentol. Sinica*, **8,** 75–83.

Manuscript received 19 September 2003; revision accepted 23 March 2004.